International Journal of Environmental Research (2026) 20:49
https://doi.org/10.1007/s41742-025-01010-3

RESEARCH PAPER

Integrated Experimental and Machine Learning Approach for Reactive Black 5 Removal Using Straw-Derived Biochars

Sabine Neusatz Guilhen[1] · Thalita Tieko Silva[1] · Guilherme Eduardo Zanetti de Sousa[1] · Sueli Ivone Borrely[1] · Leandro Goulart de Araujo[1,2]

Received: 17 July 2025 / Revised: 28 October 2025 / Accepted: 23 November 2025

Abstract

Wastewater contaminated with synthetic dyes poses significant environmental and health risks, and cost-effective solutions are urgently needed. Conventional adsorbents are often costly and exhibit limited efficiency, fostering an increasing pursuit for sustainable and economically viable alternatives. This study investigates the use of biochars derived from wheat straw (WSP), oil seed rape straw (OSR), and *Miscanthus* straw (MSP) for the removal of Reactive Black 5 dye from water. The novelty of this work lies in combining agricultural biochars with advanced data-driven approaches—including generalized linear modeling, machine learning (Random Forest, Gradient Boosting), and Monte Carlo simulations—together with ecotoxicological validation, to bridge experimental results with predictive modeling. Biochars produced at 550 °C and 700 °C were evaluated through batch adsorption experiments, FT-IR and SEM/EDS analyses, equilibrium and isotherm modeling, desorption and regeneration capabilities, and real effluent application. WSP700 achieved the highest removal efficiency (94%) at 75 g L^{-1}, with adsorption most effective at pH 5. Although higher dosages improved removal, adsorption capacity decreased due to site aggregation. Random Forest provided the best fit for capturing non-linear behavior, whereas cross-validation and external interpolation revealed that Gradient Boosting and linear/penalized regressions offered better generalization performance. Regeneration tests showed 70% desorption efficiency after seven cycles, and ecotoxicological assays revealed a marked EC_{50} increase (1.131 → 2.204), indicating reduced environmental risk. Overall, the results highlight the potential of WSP and OSR biochars as efficient, regenerable, and environmentally safe adsorbents for dye removal in wastewater treatment, supporting the development of sustainable circular-economy strategies.

✉ Leandro Goulart de Araujo
lgoulart@alumni.usp.br

[1] Nuclear and Energy Research Institute, IPEN/SP, Av. Prof. Lineu Prestes, 2242, São Paulo 05508-000, Brazil

[2] UMR 5256, Université de Lyon, Université Claude Bernard Lyon 1, CNRS, IRCELYON, 69626 Villeurbanne Cedex, France

Published online: 12 December 2025

Graphical abstract

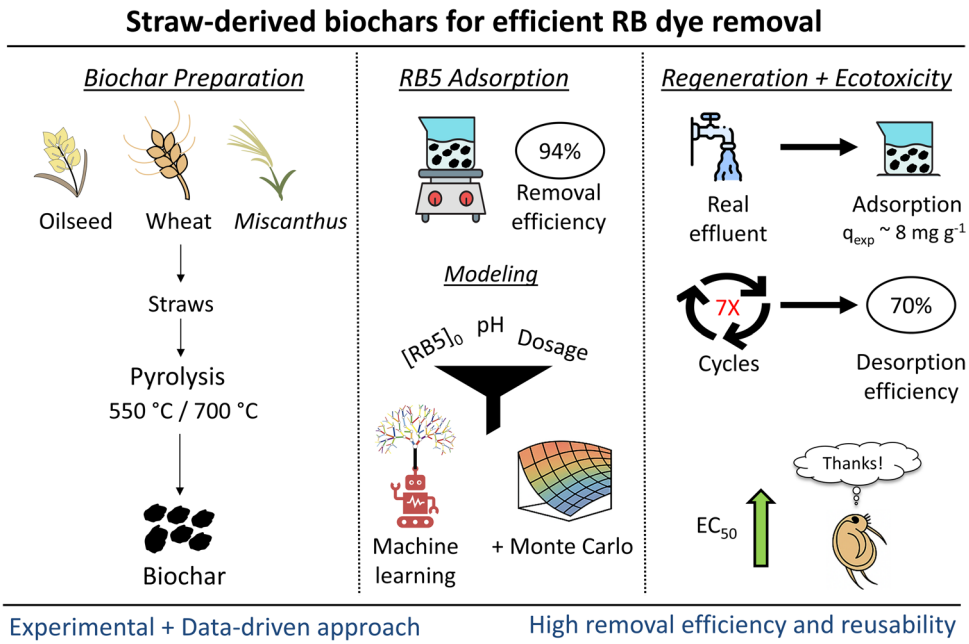

Keywords Adsorption · Dye · Wastewater treatment · Factorial design · Response surface methodology · Ecotoxicology

Abbreviations

ANOVA	Analysis of variance
ARE	Average relative error
BET	Brunauer–Emmett–Teller
DoE	Design of experiments
EC50	Half maximal effective concentration
FT-IR	Fourier-Transform Infrared Spectroscopy
GB	Gradient Boosting
ICP OES	Inductively coupled plasma optical emission spectroscopy
IDLE	Integrated development and learning environment
IS	Isotherm
LOOCV	Leave-one-out cross-validation
MC	Monte Carlo
MSP	*Miscanthus* Straw
OFAT	One-factor-at-a-time
OLS	Ordinary least squares
OSR	Oil seed rape straw
PFO	Pseudo-first order
PSO	Pseudo-second order
PZC	Point of zero charge
q	Adsorption capacity
q_m, q_{max}	Maximum adsorption capacity
RB5	Reactive Black 5
RE	Real effluent
RF	Random forest
R	Removal efficiency
RSM	Response surface methodologies
SEM/EDS	Scanning electron microscopy/Energy dispersive X-ray spectroscopy
SSA	Specific surface area
SS	Synthetic solution
TRE	Treated real effluent
TSS	Treated synthetic solution
TU	Toxic unit
URE	Untreated real effluent
USS	Untreated synthetic solution
WLS	Weighted least squares
WSP	Wheat straw

Introduction

One of the most significant issues associated with water pollution caused by the textile, plastics, leather and food industries, among others, is the release of aqueous effluents containing dyes. The dyes commonly used in these industries are resistant to biodegradation, photodegradation, and the effects of oxidizing agents. The presence of these dyes in water bodies can have a substantial negative impact on the photosynthesis of aquatic plants by reducing sunlight penetration. Furthermore, they can be toxic to fish, algae, and aquatic invertebrates due to the presence of metal substituents, chloride, aromatics, among others (Yagub et al. 2014;

Krishna Moorthy et al. 2021; Alaguprathana and Poonkothai 2021; Sari and Sari 2021).

It is estimated that around 10,000 types of dyes are produced on an industrial scale to meet the demands of the consumer market (Singh et al. 2020). Approximately 30% of the dyes produced are used in the textile industry (Dallago et al. 2005). Only a small amount of dye released as industrial effluent can have consequences for the aquatic environment, interfering with the absorption of light by plant and animal inhabitants, which may accumulate or even be transported to water treatment plants, contributing to the contamination of springs and water distributed to the population (Guaratini and Zanoni 2000).

Accurately estimate the number of various dyes released into the environment is a difficult task (Lee and Pavlostathis 2004). Most dyes not only pose a threat to aquatic organisms but also have detrimental effects on human health due to their carcinogenic, mutagenic and teratogenic properties, and respiratory toxicity (Luan et al. 2016). Azo dyes are recognized as the primary chemical class in the dyeing industry, constituting approximately 50 to 65% of commercial formulations. These dyes find application not only in textiles, but also in the pharmaceutical, food and cosmetic industries (Nigam et al. 1996; Oliveira 2005).

Among them, Reactive Black 5 (RB5) is one of the most widely used representatives. This sulfonated vinyl dye, characterized by azo groups as chromophores, has high stability and is known for its strong biological toxicity (Feng et al. 2022; Prabhakar et al. 2024). Once discharged into water bodies, RB5 can accumulate in aquatic organisms through the food chain, disrupting metabolic functions and, in severe cases, leading to mortality (Feng et al. 2022).

Several studies have sought efficient methods for removing RB5 from aqueous solutions, exploring materials such as magnetic carbons from rubber seed husks (Mokue Mafo et al. 2025), rice husk ash and powdered activated carbon (Cavalcante et al. 2024), clay and K_2CO_3-modified sludge biochar (Arif et al. 2025), as well as coagulation processes (El Idrissi et al. 2024). The chemical structure of RB5 is presented in Table 1 along with selected physicochemical properties, including molecular weight, solubility, and acid dissociation constants, which influence its environmental behavior and removal efficiency.

Given the widespread use and environmental persistence of RB5 and other azo dyes, it becomes essential to develop efficient treatment strategies for their removal from effluents. Conventional methods applied in industry include biological oxidation (activated sludge), flocculation, chemical precipitation and adsorption using activated carbon. Among these methods, the adsorption treatment approach holds great promise as it is both simple and effective in removing dyes and organic compounds from aqueous effluents (da

Table 1 Information about RB5 with its chemical structure and selected physicochemical properties. Data from (https://pubchem.ncbi.nlm.nih.gov/compound/C.I.-Reactive-Black-5; Cavalcante et al. 2024)

Chemical structure of RB5 (synonyms: Remazol Black B, Remazol Black GF)	Selected physicochemical properties	
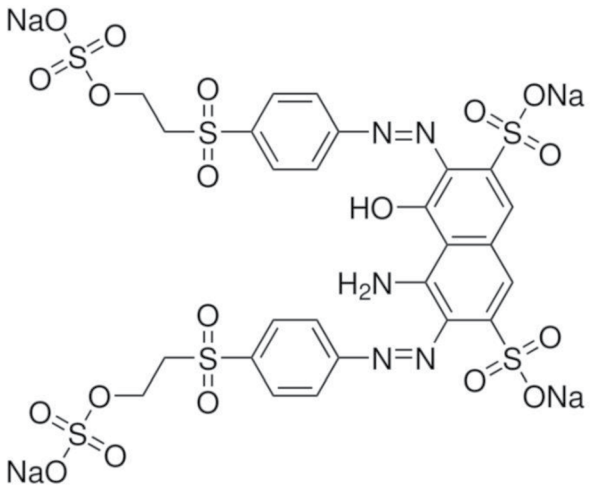	Nature	Anionic
	Dimension (nm)	1.59 × 2.55
	Molecular weight (g mol^{-1})	991.8
	pK_{a1}	3.8
	pK_{a2}	6.9
	Water solubility (g L^{-1})	550
	Hydrogen bond donor count	2
	Hydrogen bond acceptor count	24

Fontoura et al. 2017). The process of adsorption involves mass transfer from a liquid phase to a solid phase and presents significant industrial value due to its combination of low cost and high removal rates. Additionally, in certain instances, it allows for the recovery of the dye without compromising its chemical identity, making it a non-destructive process.

The most commonly used and efficient adsorbent currently available is activated carbon, which is used worldwide to remove various pollutants from water (Faria et al. 2004; Nakagawa et al. 2004; Chen et al. 2007). However, its high cost limits its use, particularly in developing countries. Therefore, it is essential to explore low-cost adsorbent materials to ensure the sustainability of the treatment process (Soares 1998). Among the promising alternatives, biochar—a carbon-rich solid obtained from the thermal decomposition of biomass—has emerged as a renewable and sustainable option.

The specific properties of biochar, including large specific surface area (SSA), porous structure, surface rich in functional groups and mineral components, make it possible to use it as a suitable adsorbent to remove pollutants from aqueous solutions. Compared to activated carbon, biochar can be an efficient and low-cost adsorbent, since its production requires lower temperatures and energy and no additional activation step (Cao et al. 2009; Zheng et al. 2010; Karakoyun et al. 2011; Lu et al. 2012; Ahmad et al. 2012). Another advantage is the abundance and low cost of its precursors, mainly agricultural biomass and solid wastes (Shen et al. 2012; Yao et al. 2012; Xu et al. 2013; Qian and Chen 2013). Thus, the conversion of biomass into biochar and its use as an adsorbent becomes an advantageous solution, both in terms of waste management and environmental sustainability (Cao et al. 2009; Zheng et al. 2010).

Numerous studies have demonstrated the excellent ability of different types of biochar to remove contaminants (heavy metals, organic pollutants, etc.) from aqueous solutions, often achieving performances comparable or even superior to commercial activated carbon (Karakoyun et al. 2011; Xue et al. 2012; Zhang et al. 2012; Yang et al. 2014). Additional investigations have confirmed its efficiency for removing various classes of organic contaminants, including dyes, pesticides, herbicides, and antibiotics (Zhang et al. 2013; Mohan et al. 2014). The utilization of agro-industrial waste for biochar production therefore represents an appealing approach, as it transforms waste materials into products with enhanced added value (Kalderis et al. 2014).

The adsorption of organic contaminants by biochar showed better data fit with the Langmuir or Freundlich models (Zhang et al. 2013; Mohan et al. 2014). The adsorption efficiency of biochar is strongly influenced by its intrinsic properties, which are largely contingent upon the production process. In addition, several parameters, including dose, initial concentration, pH, contact time, and temperature have been identified as crucial factors influencing the adsorption process (Sun et al. 2013).

In light of the aforementioned considerations, this study proposes the application of the adsorption technique to evaluate the ability of six standard biochars, derived from three different biomasses and obtained at two pyrolytic temperatures (550 °C and 700 °C), to remove the anionic dye RB5 from aqueous solutions. The effects of initial RB5 concentration, pH, and adsorbent dosage are discussed considering a detailed approach based on design of experiments (DoE) and response surface methodologies (RSM). Several mathematical models were tested against experimental data, including the Equilibrium modeling was also performed, as well as kinetic studies.

Ecotoxicological assessments with *Daphnia similis* as the model organism were conducted to evaluate the potential toxicity of RB5 in synthetic and real effluent solutions. The samples obtained before and after the adsorption tests were analyzed using Fourier-Transform Infrared Spectroscopy (FT-IR), Scanning Electron Microscopy/Energy Dispersive X-Ray Spectroscopy (SEM/EDS), and Brunauer–Emmett–Teller (BET) techniques. Finally, the practical applications of the standard biochars were demonstrated through coexisting ions completion in real effluent testing and desorption-regeneration experiments in synthetic solutions under the use of Inductively Coupled Plasma Optical Emission Spectroscopy (ICP OES) analytical measurements.

Materials and Methods

Reagents and Solutions

All solutions were prepared with analytical grade reagents and high purity water, with a resistivity of 18.2 MΩ.cm (Easypure system, model D7031, Barnstead Thermolyne, Iowa, USA). The dye solutions used in the adsorption tests were prepared from the respective stock solutions of RB5 (Sigma-Aldrich Co., San Luis, USA).

All glassware and polypropylene flasks used for the preparation and storage of samples and analytical solutions were cleaned as follows: after sequential washing with running water and deionized water, the glassware was immersed in a 10% HNO_3 bath (v/v) for 24 h. Afterwards, they were rinsed at least three times with ultrapure water. All materials were properly stored in decontaminated and covered plastic boxes.

Biochars

The standard biochars were supplied by the Biochar Research Center (UK Biochar Research Centre). They consist of biochars produced from oil seed rape straw, wheat straw and *Miscanthus* straw at two different temperatures, 550°C (OSR550, WSP550 and MSP550, respectively) and 700°C (OSR700, WSP700 and MSP700, respectively).

Adsorption Experiments

The adsorption tests were carried out in triplicate, using the batch technique. As some biochars were presented in the form of pellets, a previous grinding step were carried out in a knife mill to ensure that the tests are carried out with the same fraction. Therefore, after grinding, a granulometric separation was carried out on a 60-mesh sieve to select the fraction equivalent to particles with 250 µm.

All experiments were conducted in 100 mL beakers with a stirring rate of 130 rpm at room temperature (25 ± 2 °C). Subsequently, the mixture was subjected to centrifugation at 3,500 rpm for 15 min, after which the concentration of residual dye in solution was quantified by UV–VIS spectroscopy (Pharmacia Biotech Ultrospec 3000, Upsala, Sweden). The spectra were recorded at $\lambda_{max} = 598$ nm. The one-factor-at-a-time (OFAT) experiments were conducted to investigate the effects of varying adsorbent doses and pH, followed by the application of a DoE method. Both OFAT and DoE experiments were performed for a duration of 24 h. The calibration curve for RB5 was obtained using six points in a range of 0–100 mg L^{-1}.

The adsorption capacity of each biochar was calculated according to Eq. (1):

$$q = \frac{C_0 - C_t}{V} m \quad (1)$$

where q is the RB5 uptake (mg g^{-1}), C_0 is the initial concentration of RB5 in solution (mg L^{-1}), C is the equilibrium concentration in solution (mg L^{-1}) in a given time t, V is the volume of solution (L), and m is the mass of the biochar (g).

The extraction efficiency or retention percentage (R) was determined according to the following equation:

$$R\,(\%) = 100\frac{C_o - C_t}{C_0} \quad (2)$$

Effect of the Dose

The adsorbent's dose is deeply associated to its adsorption capacity for a given concentration of adsorbate. Experiments were performed to evaluate the dose effect of each biochar onto RB5 adsorption capacity using a 50 mg L^{-1} nominal RB5 initial concentration solution, with no pH adjustment, and varying the biochars' doses as follows: 1, 5, 10, 25, 50, 75 and 100 g L^{-1}. The doses were obtained by independently adding 0.10 g, 0.50 g, 1 g, 2.5 g, 5 g and 10 g of each biochar to 100 mL of the 50 mg L^{-1} RB5 solution.

Effect of the pH

The evaluation of the pH effect on the adsorption of RB5 is very important because the pH of the MB solutions can not only affect the degree of ionization and speciation of RB5 itself, but also affect the adsorbent's surface charge. This effect was tested by adjusting the initial dye solutions to different pH values ranging from 3 to 12 using 0.1 mol L^{-1} HNO_3 and 0.1 mol L^{-1} NaOH solutions. The pH of the RB5 solution is 7 after preparation and before any pH adjustment.

A previous study demonstrated that the pH at the point of zero charge (PZC) for the selected standard biochars were above 8.7 (Neusatz Guilhen et al. 2022), indicating that the anionic dye solution must be adjusted at < 8.7 pH values to achieve a better performance since the surface of the biochars are positively charged when $pH < pH_{PZC}$. The experiments were conducted using a 50 mg L^{-1} RB5 solution and the biochar dose selected from the previous experiment.

Two-Level Factorial Design

A number of factors such as initial concentration, pH and dose can influence the adsorption process. However, testing each of these parameters separately is time consuming, demands intensive labor, and do not allow insights about the effects on their interactions. Thus, factorial designs are useful tools since they provide empirical models that take into account not only the individual effects of each variable, but also their interactions and magnitude effects (Amini et al. 2008; Watanabe et al. 2022).

Instead of conducting a series of independent studies, the experiments are comprised in a DoE. A common DoE is based on the $n = 2^k$ equation, where n is the total of experiments, and k is the number of variables, i.e., all input factors set at two-levels each, which are defined as "high" and "low" levels. To determine the importance of each process variable in terms of maximizing RB5 removal, a full factorial design was set up considering the solution's initial concentration (C_i), pH, and the biosorbents dose (M), as shown in Table 2.

The effect of the variables was evaluated using a 2^3 factorial design (eight experimental conditions), performed in duplicates (total of 16 experimental runs), and assessed according to each parameter's low and high levels, represented by (-1) and (+1), respectively. The DoE, as well as

Table 2 Real and coded variables for *Ci*, pH, and *M*

Variables	Factor code	Low level (-1)	Middle level (0)	High level (+1)
M (g L^{-1})	A	5	7.5	10
pH	B	5	6	7
C_0 (mg L^{-1})	C	25	50	75

Table 3 Matrix of the full two-level factorial design

Test	*M* (g L^{-1})	pH	$C_{i,\,RB5}$ (mg L^{-1})
0	7.5 (0)	6 (0)	50 (0)
1	5 (-1)	5 (-1)	25 (-1)
2	10 (+1)	5 (-1)	25 (-1)
3	5 (-1)	7 (+1)	25 (-1)
4	10 (+1)	7 (+1)	25 (-1)
5	5 (-1)	5 (-1)	75 (+1)
6	10 (+1)	5 (-1)	75 (+1)
7	5 (-1)	7 (+1)	75 (+1)
8	10 (+1)	7 (+1)	75 (+1)

the statistical analysis, were processed using Python (version 3.12.7) and the Jupyter notebook as the Integrated Development and Learning Environment (IDLE) with the packages Pandas (v2.2.3) for data manipulation, NumPy (v1.26.4) for numerical operations, Statsmodels (v0.14.4) for fitting regression models and statistical analysis, and Matplotlib (v3.9.2) for generating high-resolution 3D visualizations and exporting figures. The matrix of the full factorial design of each test with their respective real and coded values are presented in Table 3. The Analysis of Variance (ANOVA) of data was carried out at a 95% confidence level to evaluate the interactions of the independent variables and the main effects on the removal percentage of RB5 and adsorption capability.

The effect of each factor and its interactions were evaluated and the result of the full factorial design is described as an adjusted linear equation that comprises the value of the outcome as a function of the factors and their interactions, as follows:

$$Y = \beta_0 + \beta_1 A + \beta_2 B + \beta_3 C + \beta_4 AB + \beta_5 AC + \beta_6 BC + \beta_7 ABC \quad (3)$$

where Y is the outcome, β_0 represents the intercept, β_i is the regression coefficient related to the interactions, and the main variables "A" is the initial concentration (mg L^{-1}), "B" is the pH value, and "C" is the adsorbent dose (g L^{-1}). Variables A, B, and C, each, represent the main effect, referring to the primary variables of interest. Variables AB, AC, BC, and ABC represent the interaction effects.

Four response variables were evaluated: Y_1 stands for RB5 removal efficiency for WSP700 (%), Y_2 is the adsorption capacity for WSP700 (mg g^{-1}), Y_3 is the RB5 removal efficiency for OSR700 (%), and Y_4 represents the adsorption capacity for the OSR700 (mg g^{-1}).

Statistical Analysis

The statistical analysis of the experimental design was performed using a quadratic RSM including linear, quadratic, and two-way interaction terms for the coded variables (dose, pH, and initial concentration, C_0). The models were fitted separately for each biochar (WSP700 and OSR700) and for each response variable (Y_1 and Y_2) using the ordinary least squares (OLS) method. Weighted least squares (WLS) regressions were additionally to include the standard deviations from replicated experiments, using the inverse of the variance ($1/\sigma^2$) as weights to account for heteroscedasticity.

Type-II ANOVA tables were generated to assess the statistical significance of each model term, with corresponding *p*-values and degrees of freedom. The goodness-of-fit metrics (R^2, adjusted R^2, AIC, BIC) and normality/homoscedasticity tests (Shapiro–Wilk and Breusch–Pagan) were computed for each model. Formal definitions of R^2, adjusted R^2, AIC, BIC are provided in Text S2 (Supplementary Information). Model assumptions were further evaluated by visual inspection of the residual plots (residuals vs. fitted values). These analyses were also performed in Python (version 3.12.7) using the statsmodels, numpy, pandas, matplotlib, and scipy libraries.

Machine Learning Workflow

Models were built separately for each biochar (no pooling and no one-hot encoding). Inputs were dose (g L^{-1}), pH, and C_0 (mg L^{-1}). Responses were $Y_1 = q$ (mg g^{-1}) and $Y_2 = R$ (%). For linear and penalized models, we used a quadratic main-effects design with all pairwise interactions: $X = \{\text{Dose, pH, } C_0, \text{Dose}^2, \text{pH}^2, C_0^2, \text{Dose} \times \text{pH}, \text{Dose} \times C_0, \text{pH} \times C_0\}$.

Predictors were standardized to zero mean and unit variance only for penalized models. We fitted OLS with intercept (statsmodels) and Ridge ($\alpha = 1.0$), Lasso ($\alpha = 0.1$), and Elastic Net ($\alpha = 0.1$, l1_ratio = 0.5) using scikit-learn. For tree ensembles (Random Forest, Gradient Boosting) we used the three original inputs (Dose, pH, C_0) without feature engineering, scikit-learn defaults, and random_state = 42. Fitting was performed per biochar using all DoE runs of that biochar.

Exploratory stress tests were implemented using the Monte Carlo (MC) method as a sensitivity check; these were not used for model selection or metrics. 10,000 scenarios were generated for each biochar by independently sampling each input from a normal distribution (μ, σ) fitted to the biochar's data and truncated at zero for feasibility. Additionally, engineered features were recomputed and

prediction distributions summarized. For OLS, we also reported a zero-bounded variant (negative predictions were set to 0).

Generalization performance was quantified within the DoE by leave-one-out cross-validation (LOOCV) on the DoE runs. We report RMSE and R^2 on the left-out folds, together with the apparent (training) fit. For interpolation, we predicted only OFAT points whose (Dose, pH, C_0) fall inside the DoE min–max envelope for the same biochar (denoted OFAT-in); these data were never used for fitting. We report external-in RMSE and R^2 when $n \geq 3$, and otherwise discuss them qualitatively. For physical plausibility, predictions used in metrics and figures were clipped to $Y_1 \geq 0$ and $0 \leq Y_2 \leq 100$. For each biochar–response, the model shown in figures was the one with the lowest LOOCV RMSE (ties broken by higher LOOCV R^2). We restrict interpretation to the DoE domain.

These analyses were also implemented in Python (statsmodels, scikit-learn, matplotlib) with random_state = 42 for stochastic procedures. Formal definitions of RMSE are provided in Text S2 (Supplementary Information).

Kinetic Study – Effect of Contact Time

Adsorption kinetics provides insight into the reaction rate and the sorption mechanism involving mass transfer, diffusion and reaction on the adsorbent surface during adsorption (Krstić 2021). After the experimental design optimization, contact time was examined from 5 min to 24 h. The pseudo-first order (PFO) equation can be written as follows (Senturk et al. 2009):

$$\ln(q_e - q) = \ln(q_e) - k_1 t \tag{4}$$

where, q_e is the amount of RB5 adsorbed at equilibrium (mg g^{-1}), q_t is the amount of RB5 adsorbed at time t (mg g^{-1}), and k_1 (min^{-1}) is the PFO rate constant. The pseudo-second order (PSO) model is described as following (Behnamfard and Salarirad 2009):

$$\frac{t}{q} = \frac{1}{k_2 q_e^2} + \frac{1}{q_e} t \tag{5}$$

where k_2 (g mg^{-1} min^{-1}) is the rate constant of the second-order equation.

Isotherm Study

Equilibrium experiments were conducted to determine the equilibrium isotherms for each biochar in the optimal operating conditions, in terms of initial concentration, pH and adsorbent dose. The adsorption isotherm is described by an equation that shows the transmission of the adsorbate from the solution phase to the adsorbent phase at the equilibrium conditions. Langmuir, Freundlich and Temkin isotherms were used to evaluate the experimental results. The linearized Freundlich adsorption isotherm is mathematically described as follows (Senturk et al. 2009):

$$\log(q_e) = \log(K_f) + \frac{1}{n}\log(C_e) \tag{6}$$

where K_F and n constants indicate adsorption capacity and adsorption intensity (L g^{-1}), respectively, and C_e is the equilibrium concentration (mg L^{-1}). Lower fractional values of n [$0 < n < 1$] suggests that weak adsorptive forces are effective on the surface of the sorbent;

Langmuir adsorption model describes the monolayer adsorption of the adsorbate on a homogeneous adsorbent surface which linear form can be described as (Tuzen et al. 2009):

$$\frac{C_e}{q_e} = \frac{1}{K_L q_m} + \frac{C_e}{q_m} \tag{7}$$

where q_e is the adsorption capacity at the equilibrium (mg g^{-1}), q_m or q_{max} is the maximum adsorption capacity calculated from the Langmuir model (mg g^{-1}), C_e is the equilibrium concentration (mg L^{-1}) and K_L is the Langmuir constant related to the energy of adsorption (L mg^{-1}).

The Temkin isotherm model assumes that the adsorption heat of all molecules decreases linearly with the increase in coverage of the adsorbent surface, and that adsorption is characterized by a uniform distribution of binding energies, up to a maximum binding energy. The linear form of the Temkin isotherm is represented by the following equation (Behnamfard and Salarirad 2009):

$$q_e = \frac{RT}{b} ln K_T + \frac{RT}{b} ln C_e \tag{8}$$

where K_T is the equilibrium binding constant (L mg^{-1}), corresponding to the maximum binding energy, b is related to the adsorption heat, R is the universal gas constant (8.314 J K^{-1} mol^{-1}) and T is the temperature (K). Plotting q_e versus $ln(C_e)$ results in a straight line of slope RT b^{-1} and intercept (RT ln K_T) b^{-1}.

The applicability of the isotherm equation to describe the adsorption process was assessed by three statistical metrics: the correlation coefficient: R^2, normalized standard deviation (NSD), and average relative error (ARE) values. R^2 was selected because it is the most widely used criterion for assessing the goodness of fit between experimental and predicted data. However, R^2 alone may not fully capture

systematic deviations, so complementary error-based metrics were also applied. ARE provides a measure of the relative deviation between experimental and model-predicted values, while NSD evaluates the dispersion of these deviations in a normalized form, allowing comparison across datasets with different magnitudes. The combined use of these three metrics ensures a more robust and reliable evaluation of model performance. The isotherm study was performed under several RB5 initial concentration values (1, 5, 10, 25, 50, 75, 100, 200, and 500 mg L^{-1}) at the equilibrium time previously selected.

Dye desorption and biochar regeneration capacity.

Three desorption tests were conducted in parallel with three different solutions: HCl 0.01 mol L^{-1}, Na_2CO_3 0.01 mol L^{-1} and NaOH 0.01 mol L^{-1}. The biochar loaded with the RB5 dye at the equilibrium concentration was placed in contact with each desorption medium under constant agitation at 130 rpm. The desorbed RB5 was registered at six intervals: 15, 30, 45, 60, 75, and 90 min. The desorption efficiency can be calculated as:

$$Desorption\,(\%) = \frac{C_{des}}{(C_{ads} + C_0)} 100 \quad (9)$$

where C_{des} (mg L^{-1}) is the desorbed dye concentration and C_{ads} (mg L^{-1}) is the adsorbed dye post-adsorption process.

Once the best desorption medium has been selected, the biochar was used to remove the same concentration of RB5 and the loss of efficiency was recorded for each cycle. The reusability of the biochar is a value-adding factor, associated with the recovery of the adsorbent (Ahmad et al. 2022). At each cycle, the same desorption medium was used to remove the adsorbed RB5 from the biochar. The experiments were interrupted when the removal efficiency dropped to half, i.e., when the material reaches its maximum reusability.

Real Effluent Application – Effect of Coexisting Compounds

Once the optimal conditions (optimized parameters) have been obtained, an assay with a real sample was performed. The real dye effluent was supplied by Instituto SENAI Corantes (São Paulo, Brazil), consisting of a mixture of dyes (Text S1) in which the RB5 is present in a concentration of 106 mg L^{-1}, total organic carbon = 82 mg L^{-1}, and at pH 11. The removal of RB5 was calculated and the impact of coexisting dyes was evaluated concerning the efficiency of RB5 removal.

Characterization

Quantitative Analysis by ICP OES

ICP OES analyses were conducted to evaluate the effect of coexisting ions present in the real effluent. The following elements were evaluated: sodium (Na), magnesium (Mg), calcium (Ca), potassium (K), strontium (Sr), and barium (Ba). The determination was performed using a PerkinElmer Optima 7000 DV spectrometer (PerkinElmer Inc., Waltham, MA, USA). The concentration ranges used for the calibration curve were as follows: Na (0.5–2.0 mg L^{-1}), Mg (0.01–0.1 mg L^{-1}), Ca (0.1–1.0 mg L^{-1}), K (0.01–0.1 mg L^{-1}), Sr (0.001–0.01 mg L^{-1}), and Ba (0.001–0.01 mg L^{-1}).

Specific Surface Area Analysis

SSA analysis was performed using a Micromeritics ASAP 2020 Plus (Micromeritics Instrument Corp, Norcross, GA, USA). The operational parameters included the use of nitrogen as the adsorptive gas at a bath temperature of -196.41 °C. The sample mass used was 1.0610 g, with warm free space and cold free space measurements of 22.7517 cm^3 and 70.5731 cm^3, respectively. The equilibration interval was set to 20 s, and automatic degassing was applied prior to analysis. The ambient temperature during the procedure was 22 °C. The procedure involved degassing the sample before analysis and measuring nitrogen adsorption and desorption isotherms to calculate the SSA using the BET model.

SEM/EDS Analysis

SEM images of the biosorbents were obtained with a Hitachi TM-3000 (Tokyo, Japan) tabletop microscope. Energy-dispersive X-ray spectroscopy (EDS) data was also collected with this equipment, with a tungsten source and acceleration voltages of 5 and 15 kV and electron beam resolution of 30 nm. Images were obtained with magnification from 500 to 1500 times. SEM allowed morphological comparison between both raw biosorbents and their loaded versions, considering that the adsorption process was carried out under optimized conditions (C_0 = 300 mg L^{-1}; pH = 5; M = 7.5 g L^{-1}; contact time = 480 min).

FT-IR Analysis

FT-IR was performed using a PerkinElmer FT-IR/NIR Frontier spectrometer (PerkinElmer Inc., Watham, MA, USA). Biochar samples were prepared as pellets using potassium bromide (Sigma-Aldrich, Merck KGaA, St. Louis, MO, USA) at a ratio of 1 mg of biochar to 400 mg of KBr. The analyses were conducted in the spectral range of 4000 to

400 cm^{-1} with a resolution of 4 cm^{-1}, and a total of 20 scans were performed.

Acute Toxicity Test

The acute effects of the samples were evaluated using *Daphnia similis* (Claus 1876; Silva et al. 2023) prior to and following treatment with WSP700 biochar. The tests were conducted using four distinct solutions. The following four solutions were utilized in the experiment: untreated real effluent (URE), treated real effluent (TRE), untreated synthetic solution (USS), and treated synthetic solution (TSS).

The exposure conditions and data analysis were conducted in accordance with the standards set forth in ABNT NBR 12.713 (ABNT 2009, p. 12). In brief, neonates (aged between 6 and 24 h) were randomly assigned to five concentrations and a negative control. All tests were conducted in a controlled chamber at 20 ± 0.5°C and a 16:8 h light:dark cycle. The organisms were not fed during the experiments. After 48 h of exposure, immobile neonates were recorded. The half maximal effective concentrations (EC_{50}) were estimated with the R-package "morse" (Baudrot and Charles 2021). Toxic unit (TU) was calculated as $TU = 100/EC_{50}$ (Ríos et al. 2017).

Results and Discussion

Effect of the Dose

The tests were performed using an RB5 solution with an initial concentration of 48 mg L^{-1} (nominally 50 mg L^{-1}), prepared in a 100 mL volumetric flask and, at this stage, no pH adjustment. The responses q (mg g^{-1}) and R (%) were calculated for six different doses and the results are displayed in Fig. 1.

The effect of the adsorbent dose on the adsorption of RB5 indicated that the removal rate increases with higher dose of biochar. This increase was more accentuated in the initial points and remained almost steady for dose higher than 25 g L^{-1}. The initial increase in the removal efficiency can be attributed to the number of adsorption sites available, which increased with the adsorbent dose.

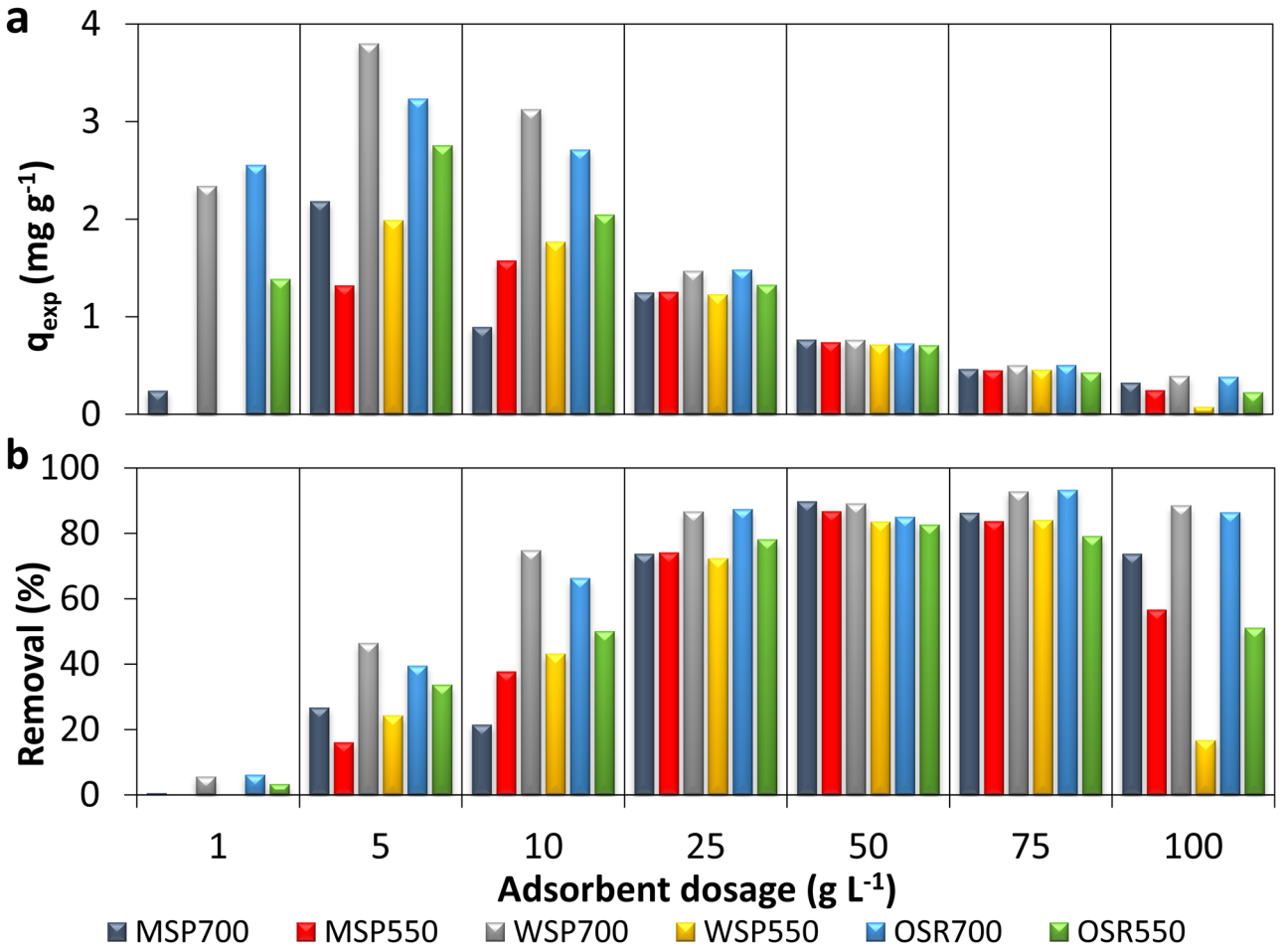

Fig. 1 Adsorption capacity (qe) and removal efficiency (R) for the six biochars using different dose

After the sites got saturated, the amount of RB5 removal reached its maximum at 75 g L^{-1} for WSP550 (85.55%) and WSP700 (94.41%), at 50 g L^{-1} for OSR550 (84.03%) and 75 g L^{-1} for OSR700 (94.96%), at 50 g L^{-1} for MSP550 (88.17%) and MSP700 (91.27%). The measurements obtained for a higher dose of 100 g L^{-1} were adversely affected because the centrifugation process was not sufficient to separate the supernatant from the biochar.

On the other hand, the total adsorbed amount of RB5 (q_{exp}) decreased as the adsorbent dose increased. This could be attributed to the aggregation or overlap of the biochar adsorption sites, due primarily to the overcrowding of the biochar particles, decreasing the total surface area available (Kuo et al. 2008; Rodrigues et al. 2011). In general, the maximum adsorption capacity (q_{max}) was obtained using a 5 g L^{-1} dose for most of the biochars, except for MSP550, for which the maximum capacity was achieved using 10 g L^{-1} (1.58 mg g^{-1}). Among the tested biochars, WSP700 achieved the highest adsorption capacity (3.80 mg g^{-1}), followed by OSR700 (3.24 mg g^{-1}), OSR550 (2.76 mg g^{-1}), MSP700 (1.32 mg g^{-1}) and WSP550 (1.99 mg g^{-1}).

The dose of 1 g L^{-1} was insufficient to provide enough sites for RB5 adsorption, whereas higher dose (>25 g L^{-1}) presented lower adsorption capacities as a consequence of partial aggregation, which occurs when a bigger amount of biochar is used, decreasing active sites (RUBIN et al. 2006). Based on these results, pH effect was assessed by selecting a uniform dose of 5 g L^{-1} for all biochars, except for MSP550, for which a dose of 10 g L^{-1} was selected.

Effect of pH

pH plays an important role in dye removal. The effect of solution pH was evaluated by varying the pH of the RB5 solutions from 3 to 12 (Fig. 2). The findings corroborated the prevailing hypothesis that pH values exceeding 8.7 ($pH > pH_{PZC}$) would impede the efficacy of the anionic dye RB5 removal process, i.e., a gradual reduction in the adsorption capacity was observed as the pH of the solution increased.

The highest adsorption capacities were achieved for WSP700 (6.08 mg g^{-1}) and OSR700 (5.48 mg g^{-1}) at pH 5,

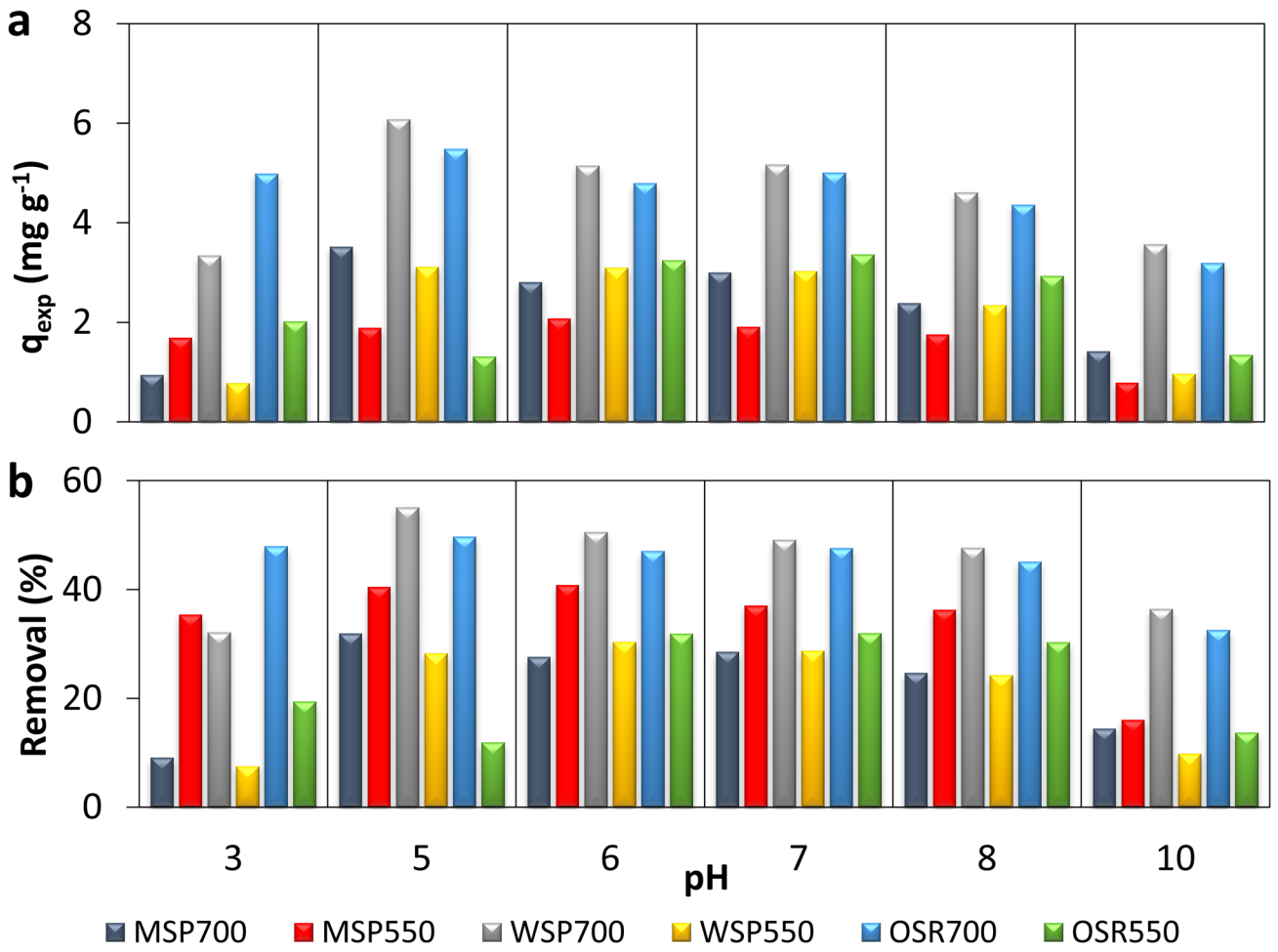

Fig. 2 Experimental adsorption capacity (qexp) and removal efficiency for the six biochars under different pH conditions

followed by MSP700 also at pH 5 (3.52 mg g^{-1}), OSR550 at pH 6 and 8 (3.24 mg g^{-1} and 3.36 mg g^{-1}, respectively), WSP550 at pH 5, 6 and 8 (3.11 mg g^{-1}, 3.09 mg g^{-1} and 3.02 mg g^{-1}, respectively), and MSP550 at pH 6 (1.91 mg g^{-1}), although at pH 5 it had a similar performance (1.89 mg g^{-1}). The pH 5 level could be selected for most of the biochars, except for OSR550, which demonstrated a superior response at pH 6 and 8.

Reactive dye anions and biochars surfaces undergo electrostatic attraction which result in the enhancement of RB5 adsorption at lower pH values ($pH < pH_{PZC} = 8.7$) (Vijayaraghavan and Yun 2008a). From these preliminary batch study with the OFAT method, pH 5 was identified to be practical and optimum for RB5 adsorption onto all of the biochars, except OSR550, for which case, a pH value between 6 and 8 could be applied. As a result, further experiments were conducted considering this pH range.

Full factorial experimental design for RB5 removal by biochar.

A full factorial design was set up for WSP700 and OSR700, considering the dose of each biosorbent (M), C_0, and the pH of the dye solution, as shown in Table 4.

Considering WSP700, the highest adsorption capacity was achieved using the test nº 5 (5.77 mg g^{-1}). Similarly, for Y_2, the optimal removal percentage occurred for the test nº 2 (93.05%). For OSR700, the results indicated a peak adsorption capacity at the experimental condition nº 0 (5.27 mg g^{-1}), while the best removal percentage was found for test nº 2 (95.89%).

Table 4 Design matrix for RB5 adsorption by WSP700 and OSR700. Y_1 stands for adsorption capacity and Y_2 stands for removal percentage

Test	M (g L^{-1})	pH	C_0 (mg L^{-1})	Y_1 (mg g^{-1})	Y_2 (%)
WSP700					
0	7.5 (0)	6 (0)	50 (0)	4.51 ± 0.01	67.34 ± 0.17
1	5 (-1)	5 (-1)	25 (-1)	3.93 ± 0.03	80.88 ± 0.54
2	10 (+1)	5 (-1)	25 (-1)	2.26 ± 0.07	93.05 ± 2.86
3	5 (-1)	7 (+1)	25 (-1)	3.63 ± 0.03	73.32 ± 0.56
4	10 (+1)	7 (+1)	25 (-1)	1.91 ± 0.10	77.22 ± 4.06
5	5 (-1)	5 (-1)	75 (+1)	5.77 ± 0.11	37.56 ± 0.71
6	10 (+1)	5 (-1)	75 (+1)	4.44 ± 0.04	57.73 ± 0.55
7	5 (-1)	7 (+1)	75 (+1)	5.32 ± 0.10	35.17 ± 0.64
8	10 (+1)	7 (+1)	75 (+1)	4.24 ± 0.12	56.08 ± 1.57
OSR700					
0	7.5 (0)	5 (0)	50 (0)	5.27 ± 0.11	73.76 ± 1.56
1	5 (-1)	4 (-1)	25 (-1)	3.76 ± 0.05	77.27 ± 1.11
2	10 (+1)	4 (-1)	25 (-1)	2.33 ± 0.01	95.89 ± 0.33
3	5 (-1)	6 (+1)	25 (-1)	3.38 ± 0.05	75.45 ± 1.13
4	10 (+1)	6 (+1)	25 (-1)	1.67 ± 0.05	74.32 ± 2.45
5	5 (-1)	4 (-1)	75 (+1)	3.06 ± 0.07	19.72 ± 0.42
6	10 (+1)	4 (-1)	75 (+1)	2.98 ± 0.06	38.33 ± 0.76
7	5 (-1)	6 (+1)	75 (+1)	4.86 ± 0.18	32.16 ± 1.19
8	10 (+1)	6 (+1)	75 (+1)	3.93 ± 0.10	52.07 ± 1.29

The Pareto graphs and surface plots in Fig. 3 highlight the relative importance of the experimental factors on RB5 adsorption by WSP700 and OSR700 biochars, as well as their interactions. These results provide mechanistic insight into how each variable influences dye removal efficiency, directly supporting the study objective of identifying optimal operating conditions for sustainable adsorbent application.

For WSP700 (Fig. 3a–b), C_0 was the most influential factor, exerting a positive effect on adsorption capacity. This suggests that WSP700 possesses a relatively high density of active sites that can accommodate increasing dye concentrations before saturation occurs (Chowdhury et al. 2011; Abdu et al. 2024). The increase in C_0 is known to enhance the concentration gradient between the liquid and solid phases, providing the driving force needed to overcome mass transfer resistance at the interface (Chowdhury et al. 2011; Goswami et al. 2022). As a result, adsorption capacity tends to rise with higher initial concentrations until the available active sites of the adsorbent are progressively saturated, at which point further increases in C_0 do not proportionally enhance uptake.

In contrast, the adsorbent dose showed a negative effect, likely due to particle aggregation at higher loadings, which reduces the effective surface area available for adsorption. The curvature of the quadratic terms further emphasizes that adsorption performance depends on the balance between these parameters. Importantly, the contour and surface plots do not reveal a true optimum within the experimental design space but instead indicate a clear directional trend: increasing adsorbent dose and maintaining a moderate C_0 would move the system toward higher adsorption capacities. This observation highlights the relevance of complementing DoE/RSM with isotherm experiments at a low WSP700 dose and increasing values of C_0 to capture the actual maximum performance of WSP700.

In the case of OSR700 (Fig. 3c–d), the adsorption behavior was more strongly governed by the quadratic effects of all three variables, resulting in a well-defined curvature in the response surface. Here, the central point of the design space lies within the region of highest adsorption capacity, meaning that the chosen experimental conditions effectively encompassed a local optimum. From a practical perspective, this underscores that OSR700 performance is sensitive to nonlinear interactions among pH, C_0, and dose, but once the system is tuned near the optimum, stable adsorption performance can be expected. For the other Pareto plots, contour plots, and 3D surface response curves, refer to Figs. S1-S4.

The strong interaction between factors and dominance of squared terms is supported by recent adsorption studies where factors such as pH, pollutant concentration, biochar dose, interact in response surface designs to define optimal dye removal (Guy et al. 2022; Rubio-Clemente et al. 2023).

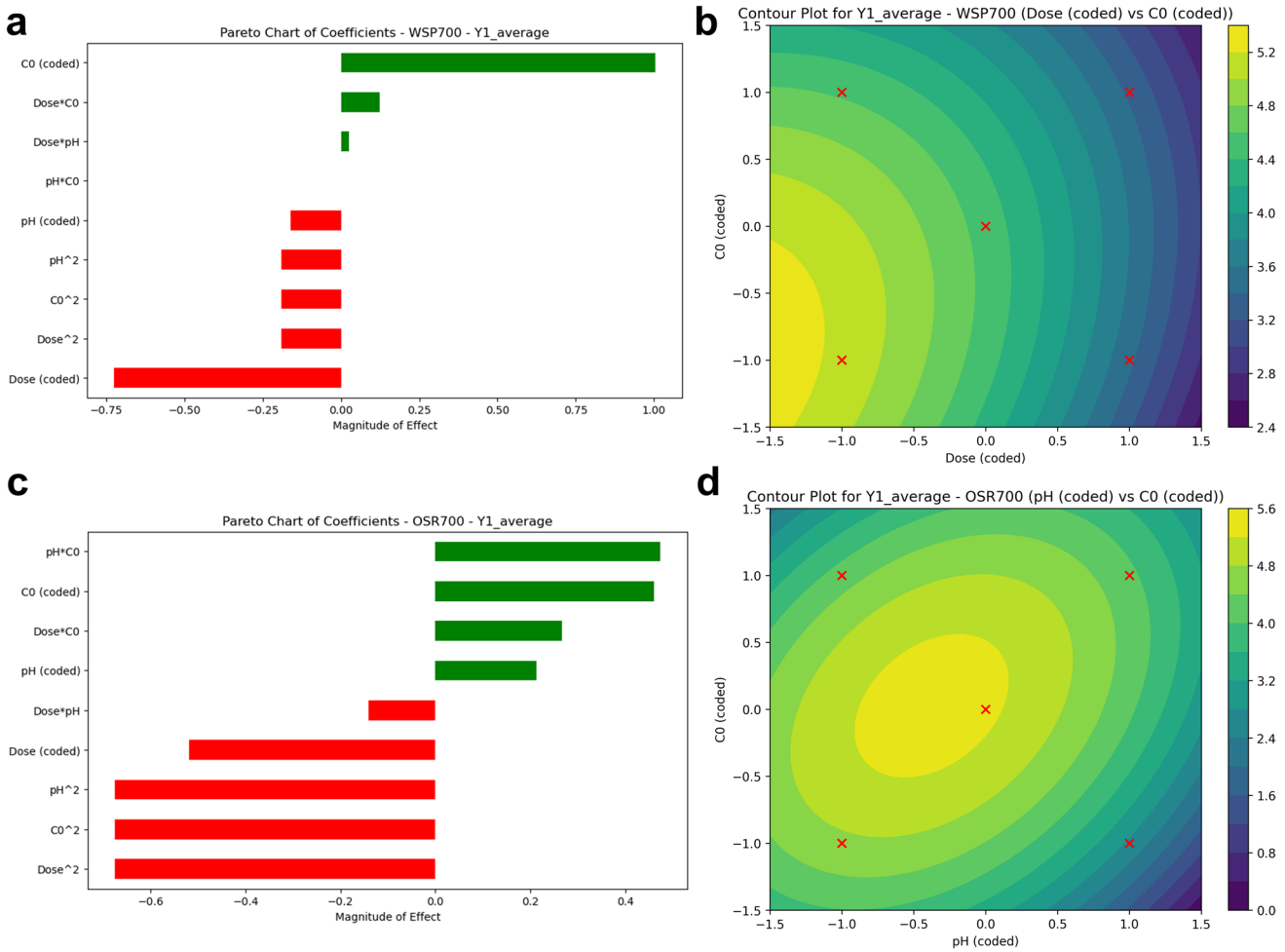

Fig. 3 **a** Pareto plot from $q_{exp,WSP700}$ regarding RB5 removal, with the most significant effects labeled (green bars: positive effect, red bars: negative effect); **b** Contour plot of the major interaction (A:C) regarding WSP700 adsorption capacity of RB5; **c** Pareto plot from $q_{exp,OSR700}$ regarding RB5 removal, with the most significant effects labeled; **d** Contour plot of the major interaction (A:B) regarding OSR700 adsorption capacity of RB5 (green bars: positive effect, red bars: negative effect)

Biochar design systems in which quadratic and interaction terms are considered can significantly improve model fits and better predict maxima.

Taken together, these results demonstrated that while WSP700 showed robust performance across a broader concentration range with C_0 and adsorbent dose as the main drivers, OSR700 exhibited a more delicate balance where interaction effects are crucial. These differences highlight how feedstock origin and pyrolysis conditions translate into distinct adsorption behaviors, underlining the importance of tailoring operational conditions to each material. The empirical models obtained (Table 5) provide a predictive framework that can guide the preliminary design of biochar-based adsorption systems for RB5-contaminated water. For detailed ANOVA tables, *p*-values, and residual plots, see Tables S1–S32 and Figs. S5–S8 in the Supplementary Material.

Although linear models are commonly employed in DoE and RSM, it is imperative to evaluate their efficacy in comparison to alternative models. As illustrated in Figs. S9-S12, the linear model demonstrated a near-perfect correlation with the experimental data, which may suggest the possibility of overfitting. In contrast, the Random Forest (RF) model demonstrated satisfactory predictive ability, although it did not precisely adhere to the ideal fit line. To assess the efficacy of both models, a MC simulation was conducted with the full equations shown in Table 5, but also for RF, as shown in Fig. 4. For gradient boosting (GB), refer to the Supplementary Material, Fig. S13.

The predicted Y_1 distributions, as illustrated in Fig. 4a and b, demonstrate notable discrepancies between the linear and RF models. The linear model displays a skewed distribution, with a higher frequency of values between 4 and 5.5 mg g^{-1}, whereas the RF model exhibits a narrower range of predicted values, with a less skewed distribution that

Table 5 Equations generated for each material and for the two target response variables. For the stepwise method, the *p*-value of 0.05 was employed

Full equation	Stepwise
$Y_{1,WSP700} = 4.5100 - 0.7250 \times Dose(coded) - 0.1625 \times pH(coded) + 1.0050 \times C_0(coded) - 0.1908 \times Dose^2 - 0.1908 \times pH^2 - 0.1908 \times C_0^2 + 0.0250 \times Dose \times pH + 0.1225 \times Dose \times C_0$	$Y_{1,WSP700} = 4.0011 + 1.0050 \times C_0(coded) - 0.7250 \times Dose(coded)$
$Y_{2,WSP700} = 67.3400 + 7.1438 \times Dose(coded) - 3.4288 \times pH(coded) - 17.2412 \times C_0(coded) - 1.1546 \times Dose^2 - 1.1546 \times pH^2 - 1.1546 \times C_0^2 - 0.9413 \times Dose \times pH + 3.1262 \times Dose \times C_0 + 2.4187 \times pH \times C_0$	$Y_{2,WSP700} = 64.2611 - 17.2412 \times C_0(coded) + 7.1438 \times Dose(coded)$
$Y_{1,OSR700} = 5.2700 - 0.5187 \times Dose(coded) + 0.2138 \times pH(coded) + 0.4613 \times C_0(coded) - 0.6746 \times Dose^2 - 0.6746 \times pH^2 - 0.6746 \times C_0^2 - 0.1413 \times Dose \times pH + 0.2662 \times Dose \times C_0 + 0.4737 \times pH \times C_0$	$Y_{1,OSR700} = 3.4711$
$Y_{2,OSR700} = 73.7600 + 7.0013 \times Dose(coded) + 0.3487 \times pH(coded) - 22.5812 \times C_0(coded) - 5.2029 \times Dose^2 - 5.2029 \times pH^2 - 5.2029 \times C_0^2 - 2.3063 \times Dose \times pH + 2.6287 \times Dose \times C_0 + 6.1962 \times pH \times C_0$	$Y_{2,OSR700} = 59.8856 - 22.5812 \times C_0(coded)$

aligns more closely with the experimental range than that observed in the linear model. For all predictions, including both materials and response variables, as well as the MC tests, refer to the Supplementary Material (Figs. S9–S17).

The linear model's capacity for extrapolation beyond the experimental range renders it a valuable tool for identifying exceptional materials (Kauwe et al. 2020). Nonetheless, the assumption of linearity frequently engenders inherent issues in models when confronted with multicollinearity or nonlinear data, in addition to the hypothesis of independence with respect to predictors (De Araujo et al. 2025). This extrapolation can also result in implausible values, such as negative adsorption capacities. In contrast, the RF model exhibits a more constrained range of predicted values, rendering it less susceptible to unrealistic predictions and more consistent with the experimental data range.

Figure 4c-d depict the distribution of predicted Y_1 values for WSP700 in relation to dose and C_0. The top 25% of values are indicated in red, with the yellow fill representing the highest predicted values. The linear model's prediction map for Y_1 and WSP700, as illustrated in Fig. 4c, appears to encompass a considerably broad dose range, from 2.5 to 10 g L^{-1}. In contrast, for RF (Fig. 4d), these values are concentrated at lower doses and higher C_0 values, suggesting that working with doses between 4 and 5.5 g L^{-1} and C_0 values above 60 mg L^{-1} can achieve the highest RB5 adsorption capacities for WSP700. GB shows a greater degree of experimental variability at the 25% higher values, even reaching zero values for the dose, which is not a realistic outcome (Fig. S13).

These differences further corroborate the potential for overfitting discussed earlier. While the linear model can serve as a benchmark when aiming for optimized parameter values, RF is more suitable for avoiding overfitting and operating within a more restricted, realistic prediction range. We emphasize that MC does not validate models; it stress-tests them within the assumed input variability. MC is informative (stress-testing) rather than confirmatory.

Model Validation and Scope

Given the limited number of experimental conditions per biochar in the DoE, highly flexible machine learning algorithms are prone to overfitting, yielding over-optimistic apparent fits and poor generalization to unseen data. While large datasets can mitigate this risk, that is not the case in this particular study. Generalization within the experimental domain was quantified by LOOCV on the DoE and by an external interpolation check using only OFAT points that lie inside the DoE envelope (min–max in Dose, pH, C_0) for the same biochar (see Table S33). For WSP700, four OFAT points met this in-domain criterion and were retained for

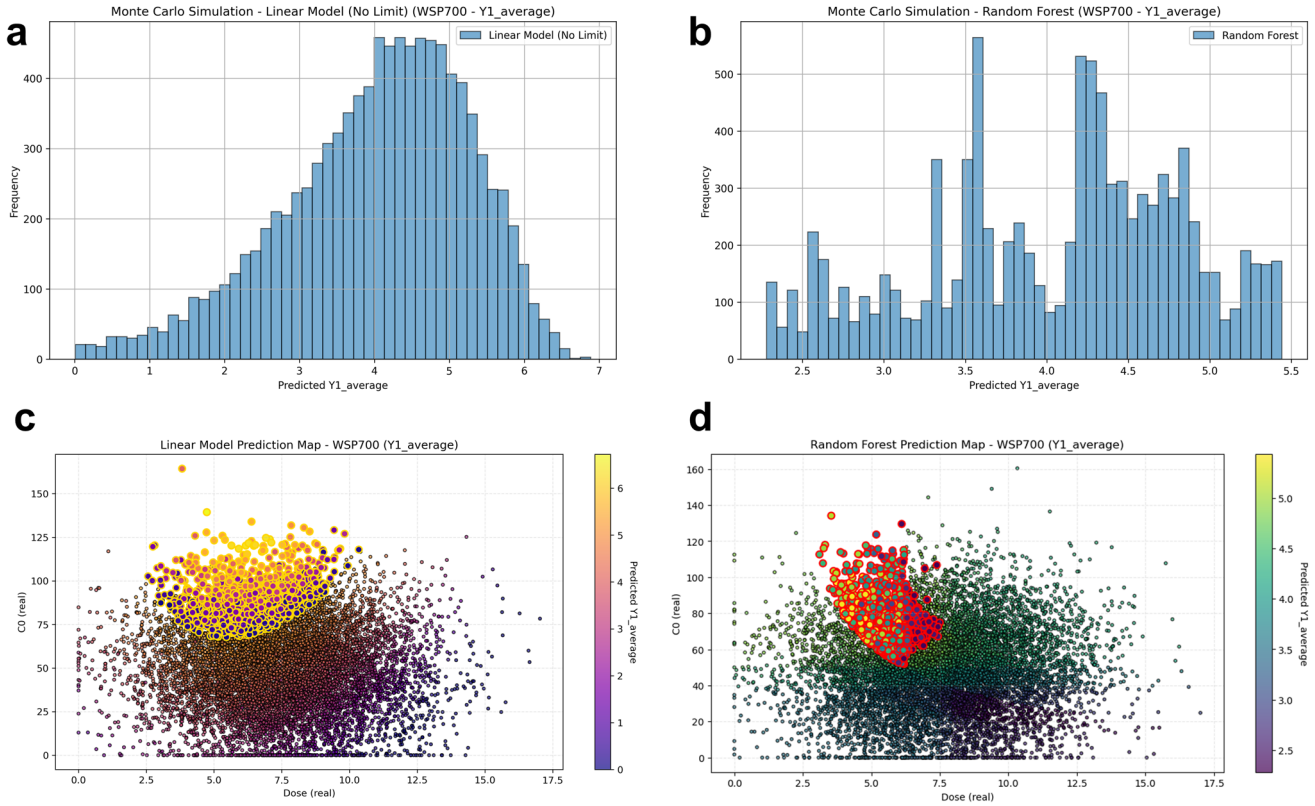

Fig. 4 Modeling of RB5 adsorption with WSP700 as the adsorbent. Distribution of data outputs by applying Monte Carlo simulation with the models from **a** linear regression, **b** random forest; Distribution of predicted Y_1 values by applying wide ranges for Dose and C_0 with the **c** linear regression, **d** random forest

external testing; for OSR700, only two OFAT points were in-domain, which is insufficient for a stable estimate of external R^2 and RMSE, so these values are reported qualitatively (see Table S34).

For Y_1 (q, mg g^{-1}), GB achieved the lowest LOOCV RMSE and showed consistent interpolation on OFAT-in for WSP700, indicating mild nonlinearity within the DoE. For Y_2 (R, %), linear/penalized models outperformed ensembles, providing stable generalization with fewer degrees of freedom. In WSP700, the best model (selected by lowest LOOCV RMSE) yielded high LOOCV performance for Y_1 ($R^2 = 0.94$, RMSE = 0.30) and moderate-to-high performance for Y_2 ($R^2 = 0.82$, RMSE = 7.85%), consistent with parity plots (Fig. S18). In OSR700, LOOCV performance for Y_2 was moderate ($R^2 = 0.65$, RMSE = 14.25%), whereas Y_1 showed limited generalization (positive LOOCV R^2 only for GB; $R^2 = 0.57$, RMSE = 0.70). This pattern reflects the sparse design (nine runs) and the stronger leverage of individual points on Y_1.

Three factors likely contribute to the weaker generalization for OSR700 Y_1: (i) high leverage under small-n LOOCV; (ii) response curvature for q not fully captured by quadratic terms within the available span; and (iii) measurement noise, which inflates evaluation variance. Methodologically, these issues would be best addressed by augmenting the DoE (additional central/edge points) or, alternatively, by pooling across related feedstocks/temperatures via hierarchical modeling—both beyond the scope of the present study, which keeps models per biochar.

Overall, within the constraints of the dataset, simple linear/penalized models trained on DoE generalize best to in-domain conditions and provide transparent response surfaces. Ensemble models show no consistent advantage at n ≈ 10. The OFAT-in check supports the use of DoE-trained linear baselines and a nonlinear model for WSP700's Y_1, and highlights the scope of inference as interpolation within the DoE envelope rather than extrapolation.

Kinetic Study – Effect of Contact Time

The kinetic study of RB5 dye removal using two different biochars, WSP700 and OSR700, was analyzed using both PFO and PSO kinetic models (Fig. 5). The equilibrium was reached within 480 min for both adsorbents.

The parameter values are presented in Table 6. For WSP700, the PFO model yielded a q_e value of 5.56 mg g^{-1} with a rate constant k_1 of 0.0087 min^{-1} and an R^2 of 0.96, indicating a good fit to the experimental data. The PSO

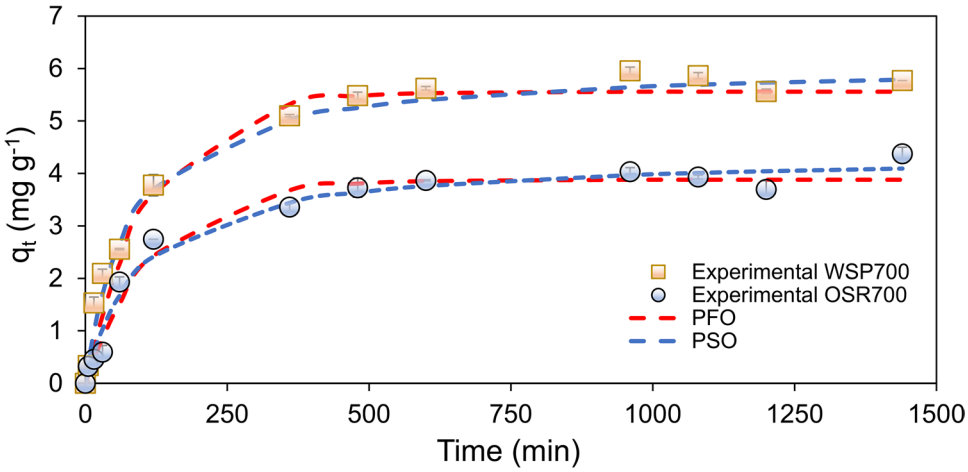

Fig. 5 Kinetic models of RB5 adsorption onto WSP700 and OSR700 (Eqs. 4 and 5)

Table 6 Kinetic parameters calculated for RB5 removal for WSP700 and OSR700

Material	Model	Parameter	Value	R^2
WSP700	PFO	q_e (mg g^{-1})	5.56	0.96
		k_1 (min^{-1})	0.0087	
	PSO	q_e (mg g^{-1})	6.10	0.98
		k_2 (g mg^{-1} min^{-1})	0.0021	
OSR700	PFO	q_e (mg g^{-1})	3.88	0.97
		k_1 (min^{-1})	0.0082	
	PSO	q_e (mg g^{-1})	4.37	0.98
		k_2 (g mg^{-1} min^{-1})	0.0023	

model provided a higher q_e value of 6.10 mg g^{-1} and a rate constant k_2 of 0.0021 g mg^{-1} min^{-1} with an R^2 of 0.98, suggesting an even better fit.

The higher R^2 value for the PSO model compared to the PFO model implies that the adsorption process for WSP700 is better described by the PSO model. This suggests that the rate-limiting step is likely chemisorption, involving valence forces through sharing or exchange of electrons between the adsorbent and the adsorbate.

For OSR700, the PFO model resulted in a q_e value of 3.88 mg g^{-1} and a k_1 of 0.0082 min^{-1} with an R^2 of 0.97, indicating a good correlation with the experimental data. The PSO model showed a q_e value of 4.37 mg g^{-1} and a k_2 of 0.0023 g mg^{-1} min^{-1} with an R^2 of 0.98. Similar to the WSP700 material, the PSO model provided a superior fit for the OSR700, as evidenced by the higher R^2 value compared to PFO. This suggests that chemisorption is also the predominant mechanism for the adsorption of RB5 dye onto the OSR700.

When comparing the two biochars, WSP700 exhibits a higher adsorption capacity (q_e) than OSR700 in both kinetic models. This suggests that WSP700 is more effective in removing RB5 dye from aqueous solutions. The rate constants for both models are slightly higher for WSP700 than for OSR700, indicating a marginally faster adsorption process for WSP700. Both materials reached adsorption equilibrium in 480 min, which underscore their practical applicability in treatment processes.

Overall, the kinetic data suggest that both biochars follow the PSO model more closely, implying that chemisorption is the dominant mechanism for RB5 dye removal. This suggests that adsorption involves valence forces through electron sharing or exchange between dye molecules and surface functional groups such as hydroxyl, carboxyl, and aromatic π-electrons. In addition to this chemical interaction, electrostatic attraction also plays an important role. The pH-dependent adsorption behavior supports this dual mechanism: under acidic to neutral conditions (pH < pH_{PZC} = 8.7), protonation of the biochar surface enhances electrostatic attraction with the anionic sulfonate groups of RB5. Similar results were reported by Hamzeh et al. (2012), who demonstrated that adsorption of reactive dyes on lignocellulosic sorbents occurs through the combined action of electrostatic attraction and chemical bonding with the adsorbent functional groups. Although the PSO model adequately described the adsorption kinetics observed in this study, its applicability has limitations. The model may show poor predictivity in some systems. For instance, in systems where mass transfer is rate-limiting, such as when external film diffusion or intraparticle diffusion dominates, the PSO model may not accurately describe the initial adsorption rates. Similarly, for heterogeneous sorbent surfaces with multiple adsorption sites of varying affinities, the single-site assumption inherent to the PSO model can lead to deviations from experimental data. Additionally, under very high or very low solute concentrations, the linearization of the PSO model may fail, reducing predictive accuracy (Hubbe et al. 2019). Therefore, while the PSO model is a useful and widely applied tool for describing batch adsorption kinetics, its reliability should be evaluated on a case-by-case basis, considering sorbent properties and experimental conditions.

The superior performance of WSP700 compared to OSR700 in terms of both adsorption capacity and rate

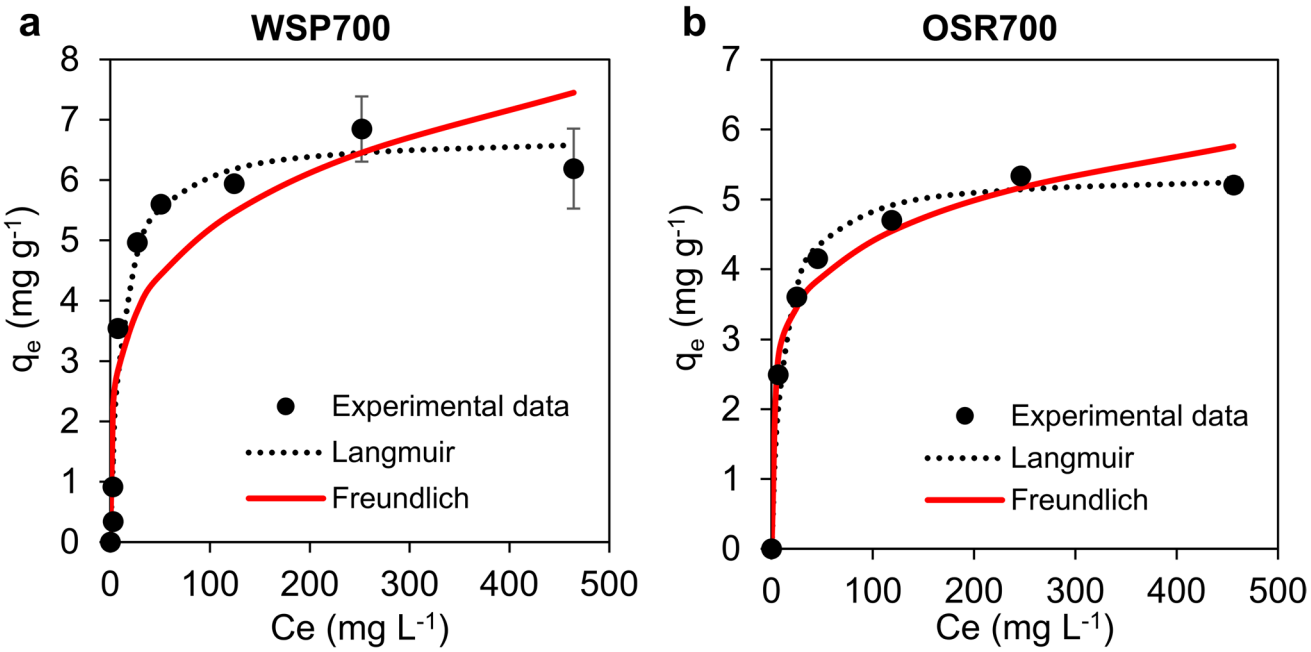

Fig. 6 Non-linear isotherms of WSP700 and OSR700 during RB5 adsorption

Table 7 Parameters calculated by using the Langmuir and Freundlich adsorption isotherm models for RB5 adsorption on WSP700 and OSR700, along with the corresponding correlation coefficients obtained for each model

Material	Models	Parameters			
WSP700	Langmuir	q_{max}	6.74	R^2	0.944
		K_L	0.09		
	Freundlich	n	4.26		0.751
		K_F	1.76		
OSR700	Langmuir	q_{max}	5.37	R^2	0.999
		K_L	0.09		
	Freundlich	n	5.68		0.931
		K_F	1.96		

constants highlights its potential as a more efficient adsorbent for RB5 dye removal in wastewater treatment applications.

Isotherm Studies

The adsorption data for RB5 onto WSP700 and OSR700 were analyzed using Langmuir and Freundlich isotherm models to evaluate the adsorption capacity and adsorption phenomenon. The results are displayed in Fig. 6 and the parameters are described in Table 7.

The high R^2 values for both materials indicate a strong fit to the Langmuir model, suggesting that the RB5 adsorption onto these adsorbents predominantly occurs as monolayer adsorption on homogeneous sites.

The Freundlich model also supports the occurrence of adsorption on heterogeneous surfaces, albeit with a less precise fit (lower R^2 values) than the Langmuir model. This suggests that the Langmuir model better represents the adsorption process for both adsorbents.

The SSA values for WSP700 (11 m^2 g^{-1}) and OSR700 (5 m^2 g^{-1}) directly correlate with their respective adsorption capacities, as WSP700's higher SSA likely provides more active sites for adsorption, facilitating the interaction between the biochar surface and dye molecules. This is consistent with the Langmuir model's prediction, which indicate a higher q_{max} for WSP700 (6.74 mg g^{-1}) compared to OSR700 (5.37 mg g^{-1}), highlighting its superior effectiveness in RB5 adsorption.

The comparison between WSP700 and OSR700 shows that WSP700 has a higher q_{max} for RB5 than OSR700, indicating that WSP700 is more effective in adsorbing RB5. The Langmuir constants K_L for both materials are relatively similar, indicating similar adsorption energies.

Desorption-Regeneration Experiments

The results of the desorption experiments are presented in Fig. 7. This test was specifically applied to WSP700, as it demonstrated the best performance in the adsorption of RB5. Given WSP700's high adsorption efficiency, understanding its desorption behavior was crucial to evaluate its potential for regeneration and reuse in multiple adsorption–desorption cycles.

As can be seen in Fig. 7a, Na_2CO_3 was the best desorption medium, since it was able to achieve a higher desorption efficiency when compared to other solutions within the same time intervals, indicating that Na_2CO_3 is more

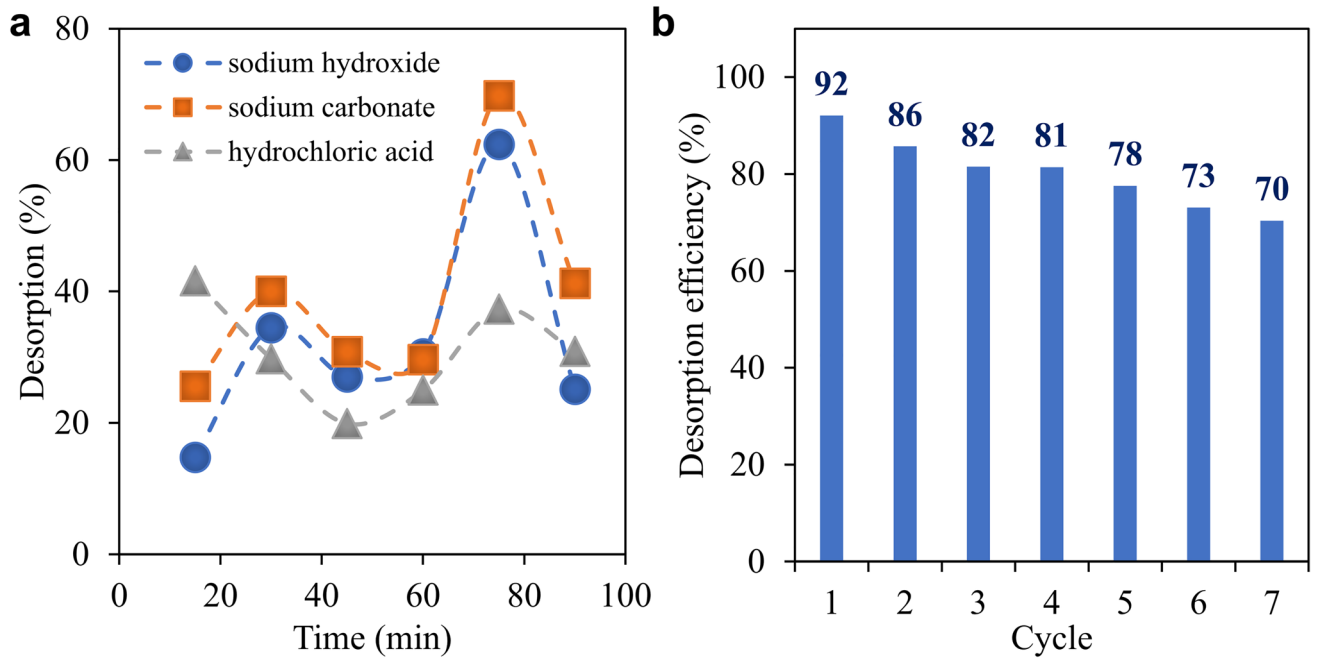

Fig. 7 **a** Desorption efficiency of different desorption media. **b** Regeneration results over seven cycles by employing Na_2CO_3 as the desorption medium

effective at breaking the adsorbate-adsorbent bonds compared to the other solutions. This suggests that Na_2CO_3 has a stronger interaction with the active sites on the adsorbent surface, facilitating the release of the adsorbed species more efficiently. Additionally, its higher desorption efficiency implies that it could be a preferred choice for the regeneration of WSP700 in repeated adsorption–desorption cycles, potentially enhancing the material's reusability and cost-effectiveness in practical applications.

The results of regeneration experiments are shown in Fig. 7b. The experiments were conducted over seven cycles, demonstrating that a removal efficiency above 70% was still achievable by the final cycle. This highlights the economic and practical potential of WSP700 biochar as an adsorbent for RB, with adequate renewability for multiple uses. In the first cycle, the removal efficiency was 92.04%, followed by 85.69% in the second, 81.51% in the third, 81.40% in the fourth, 77.57% in the fifth, 73.07% in the sixth, and 70.37% in the seventh. This reflects a reduction in removal efficiency of approximately 23.54% from the first to the last cycle, indicating strong regeneration capability across multiple cycles with minimal performance loss.

Effect of Coexisting Ions

The results of the ICP OES analysis for the real effluent, detailing the major elements, show the presence of sodium (Na), magnesium (Mg), calcium (Ca), potassium (K), strontium (Sr), and barium (Ba), with concentrations in mg L^{-1} as follows: Na (1.694), Mg (0.081), Ca (0.557), K (0.054), Sr (0.003), and Ba (0.002). Although the presence of these coexisting ions could theoretically affect the adsorption, it is important to note that RB5 is an anionic dye. As an anion, it does not directly compete with the cations in the effluent for adsorption sites. Additionally, the cations were found in very low concentrations, which will likely have no observable effect on RB5 adsorption onto WSP700.

It is worth mentioning, however, that higher concentrations of cations could potentially alter the electrostatic interactions between the dye and the adsorbent's surface. Given that the real effluent has a pH of 10, the biochar's surface would be negatively charged. In such conditions, an increase in ionic strength due to higher cation concentrations could reduce electrostatic repulsion between negatively charged species, thereby enhancing adsorption (Aranda-García et al. 2020). Furthermore, the cations (Na^+, Mg^{2+}, Ca^{2+}, etc.) found in the real effluent, even at low concentrations, may have modulated the ionic strength of the medium (Fu et al. 2023).

This modulation can reduce electrostatic repulsion for the cations by forming a neutralizing layer around the biochar, decreasing the repulsion between RB5 and the negatively charged surface of WSP700. Thus, the effect of coexisting ions is not always detrimental; under certain circumstances, their presence could positively influence the adsorption process by mitigating electrostatic repulsion and facilitating the interaction between the dye and the adsorbent.

Real Effluent Application

The optimized parameters for the adsorption process were applied to a real RB5 effluent sample to evaluate the effect of coexisting ions in a mixed solution. For this test, the adsorption experiment was conducted directly on the real effluent without pH adjustment, which was initially measured at 10. This setup aimed to assess the adsorption performance of WSP700 as an adsorbent for RB5 under actual effluent conditions, leveraging the optimized parameters determined for maximum efficiency.

Simultaneously, a simulated RB5 solution was prepared at approximately 100 mg L^{-1}, matching the concentration found in the real effluent. This parallel test allowed for direct comparison between the adsorption efficiency in real effluent and in a controlled, single-component solution. Notably, in the real effluent, the adsorption capacity of WSP700 was calculated to be 7.76 mg g^{-1}, with a corresponding RB5 removal efficiency of 32.65%, similar to the behavior observed in the synthetic solution (under same experimental conditions), indicating that the adsorption performance is not significantly influenced by the additional constituents present in the real effluent. This finding suggests that WSP700 is resilient to potential competitive adsorption effects from other ions and compounds typically present in industrial dye effluents, making it a promising adsorbent for practical applications in wastewater treatment.

Although WSP700 exhibited relatively moderate q_{max} (Langmuir = 9.45 mg g^{-1}) compared to chemically modified adsorbents and activated carbons reported in the literature, this observation can be explained by the experimental conditions, the intrinsic material properties (BET ≈ 11 m^2 g^{-1}), and the complexity of the real effluent tested. Many of the highest q_{max} values are reported for highly functionalized materials (e.g., crosslinked chitosan) or microporous carbons, which are not directly comparable to non-activated biochars derived from agricultural residues. Moreover, the dose effect observed in our experiments—where q decreased at high doses due to particle aggregation—suggests that removal efficiency under realistic operating conditions is a more practical indicator of performance than q_{max} alone. In this respect, WSP700 demonstrated high removal efficiency (94% at 75 g L^{-1} in synthetic solution) and good reusability (≈70% after seven cycles). Combined with its low production cost and sustainability, these features highlight the potential of WSP700 as a low-cost adsorbent for pre-treatment or polishing stages, with room for further improvement through physical or chemical activation.

A comparison between our results and those reported in the literature is presented in Table 8, which compiles q_{max} and other relevant parameters such as equilibrium times and desorption efficiencies. This table highlights the scarcity of studies employing real effluent solutions and including desorption evaluations, underscoring the practical relevance of the present findings.

SEM/EDS Analysis

The morphological characteristics of WSP700 before and after the adsorption process were examined using SEM (Fig. 8). Figures 8a, b illustrates the SEM image of pristine WSP700 biochar before adsorption of RB5, which structure exhibited a smooth, porous surface, with striations, typical of carbon-based adsorbents. This porous morphology likely results from the breakdown of lignocellulosic biomass at elevated temperatures during pyrolysis, causing the evaporation of volatile compounds and the formation of pores, as reported in similar studies (Arafat Hossain et al. 2017; Kong and Liu 2021; Zhang et al. 2023). The presence of these pores provides an extensive surface area, favorable for the adsorption of pollutants.

After adsorption of the synthetic dye solution (Fig. 8c, d), significant changes in the surface morphology were observed. The biochar's surface became more heterogeneous and coarser, exhibiting a rough microstructure while retaining its porous structure, which provides ample binding sites for dye molecules.

FT-IR Analysis

The comparative FT-IR spectra of WSP550 and WSP700 biochars are presented in Fig. 9a, followed by the spectra of WSP700 before and after the adsorption of RB5, as shown in Fig. 9b.

The FT-IR analysis of WSP550 and WSP700 highlights smooth changes in functional group intensities and compositions due to the difference in the pyrolysis temperature at which each of these biochars was obtained. The broad band between 3500 cm^{-1} and 3300 cm^{-1} associated with O–H of hydroxyl functional phenolic groups, including hydrogen bonding due to adsorbed water, exhibited a marked reduction in WSP700, indicating the loss of hydroxyl groups and residual moisture as pyrolysis progressed (Vaghela et al. 2023; Ćwieląg-Piasecka et al. 2023). Similarly, peaks in the aliphatic C–H stretching region (3040–2850 cm^{-1}), prominent in WSP550, were nearly imperceptible in WSP700, reflecting the thermal degradation of aliphatic structures derived from cellulose, hemicellulose, and lignin (Elnour et al. 2019). These observations are consistent with the progressive volatilization and decomposition of organic compounds at higher temperatures.

Further structural modifications were evident in the aromatic and polysaccharide-associated regions. An intense band at 1580 cm^{-1}, related to the vibrations of aromatic

Table 8 Comparison of maximum adsorption capacities (qmax) in the literature considering other bio-based and commercial adsorbents used for RB5 removal. SS: synthetic solution, RE: real effluent, IS: isotherm. Unless otherwise indicated, assume that SS is the solution used

Material	qmax (mg g-1)	R (%)	Eq. time	Kinetics	Isotherm	References	Desorption
WSP700	6.74 (SS-IS), 7.76 (RE)	93.05 (DoE), 32.65 (RE)	480 min (SE)	PSO (SE)	Langmuir (SE)	This study	70.37% after seven cycles Na2CO3 0.01 mol L-1
OSR700	5.37 (SS-IS)	95.89 (DoE)	480 min (SE)	PSO (SE)	Langmuir (SE)		
Modified natural zeolite	0.0691	-	300 min	PSO	Langmuir	(Lestari et al. 2023)	No
Clay residue	0.98	-	5 min	-	Langmuir	(Silva et al. 2018)	No
Brazilian pine-fruit shells (Araucaria angustifolia)	74.6	55.6 (simulated dye mixture effluent at pH 2.0)	12 h	Avrami	Sips	(Cardoso et al. 2011)	No
Activated carbon derived from the Brazilian pine-fruit shells (Araucaria angustifolia)	446.2	94.3 (simulated dye mixture effluent at pH 5.8)	4 h	Avrami	Sips		
Leclercia adecarboxylata	278.40	97.4	60 min	PSO	Hill	(Şen et al. 2025)	No
Templated crosslinked-chitosan	2941	-	-	PSO	Langmuir	(Chen and Huang 2010)	Yes
Microporous activated carbon felt	21	-	110 h	Intra-particle diffusion	Khan and Langmuir–Freundlich	(Donnaperna et al. 2009)	No
GLA-crosslinked-chitosan, homogeneous coupling, using NaOH	1680	-	-	PSO	Langmuir	(Chen and Chen 2009)	58% desorption efficiency after first cycle using NaOH at pH 12
Chitosan/amino resin and chitosan bearing both amine and quaternary ammonium chloride moieties (two resins)	625–932	-	50 min	PSO	Langmuir	(Elwakeel 2009)	96–97% desorption efficiency for 3 cycles using NH4OH/NH4Cl (pH 10) buffer
Acid-treated biomass of brown seaweed Laminaria sp.	101.5	72.7 (up-flow packed column)	3 h	PSO	Langmuir	(Vijayaraghavan and Yun 2008b)	97.7% desorption efficiency using NaOH 0.01 M
Live activated sludge	134.8	82.3	30 min	PSO	Sips	(Aksu and Akın 2010)	No
Dried activated sludge	126.5	78.0	30 min	PSO	Sips		
NaOH-treated activated sludge	123.1	69.0	30 min	PSO	Sips		
Sugar beet pulp carbon	80	14.6 (real wastewater)	180 min	PSO	Langmuir	(Dursun et al. 2013)	No
Dried-orange peel	62.4	31.4 (max)	2–4 h	PSO	Langmuir	(Karaman and Aksu 2020)	No
Chemically modified orange peel	84.4	38.5 (max)	2–4 h	PSO	Langmuir		
Cotton plant stalk	35.7	54.9 (Ci = 25 mg L-1)	3–5 h	PSO	Langmuir	(Tunç et al. 2009)	No
Cotton plant hull	50.9	79.6 (Ci = 25 mg L-1)	3–5 h	PSO	Langmuir		
Green coconut mesocarp	2.93	-	1 h	-	Langmuir	(Leal et al. 2010)	No

Table 8 (continued)

Material	qmax (mg g-1)	R (%)	Eq. time	Kinetics	Isotherm	References	Desorption
Rhizopus arrhizus	588.2	90.2—53.4 (Ci = 17.7 – 428.9 mg L-1, 25 ºC)	30–120 min Ci = 80—400 mg L-1)	PSO	Freundlich	(Aksu and Tezer 2000)	No
Lewatit MonoPlus MP 62	796.1	75.2	24 h	-	Langmuir	(Wawrzkiewicz and Hubicki 2011)	95% desorption efficiency using 1 M KSCN in 40–60% methanol, 1 M
Bacterial cellulose	17.5	92	80 min	PSO	Langmuir	(Leal et al. 2021)	No
Canola stalks	32.8	93.6 (dose of 10 g L-1, pH 3)	30 min	PSO	Langmuir	(Ashori et al. 2012)	No
Bagasse	7.51	-	15 min	PSO	Langmuir	(Ziapour et al. 2016)	No

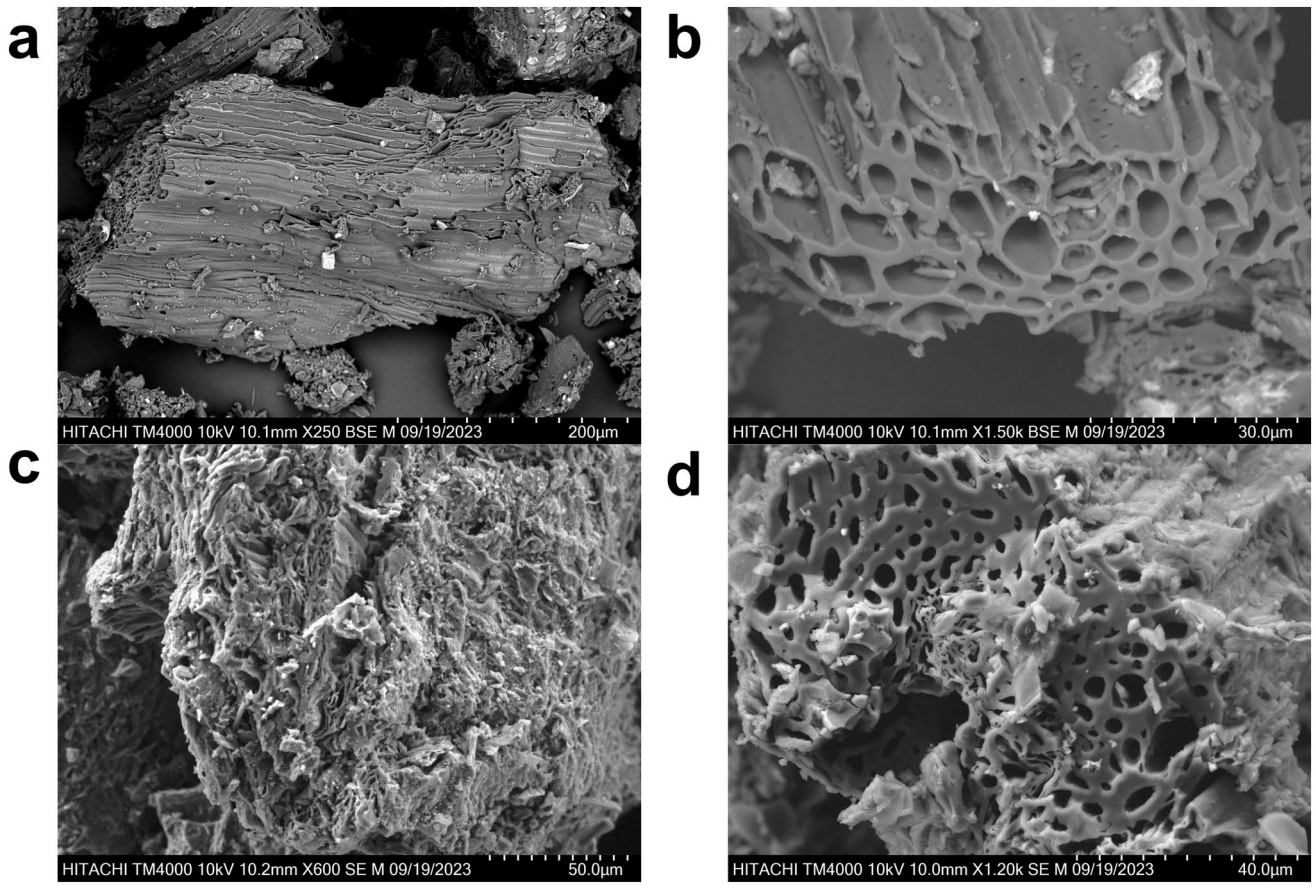

Fig. 8 SEM images for WSP700 biochar **a**, **b** before adsorption; **c**, **d** after RB5 adsorption with the synthetic solution

C = C and C = O groups of conjugated ketones and quinones (Manna et al. 2020), diminished in WSP700, suggesting a transition toward more condensed and thermally stable aromatic structures. The absence of the C–H bending peak at 1375 cm^{-1} and the reduced intensity of C–O stretching in the 1084–1100 cm^{-1} band confirm the breakdown of polysaccharides and aliphatic chains (Qayyum et al. 2012). These spectral transformations underscore the increased aromaticity and carbonization of the biochar as pyrolysis temperature

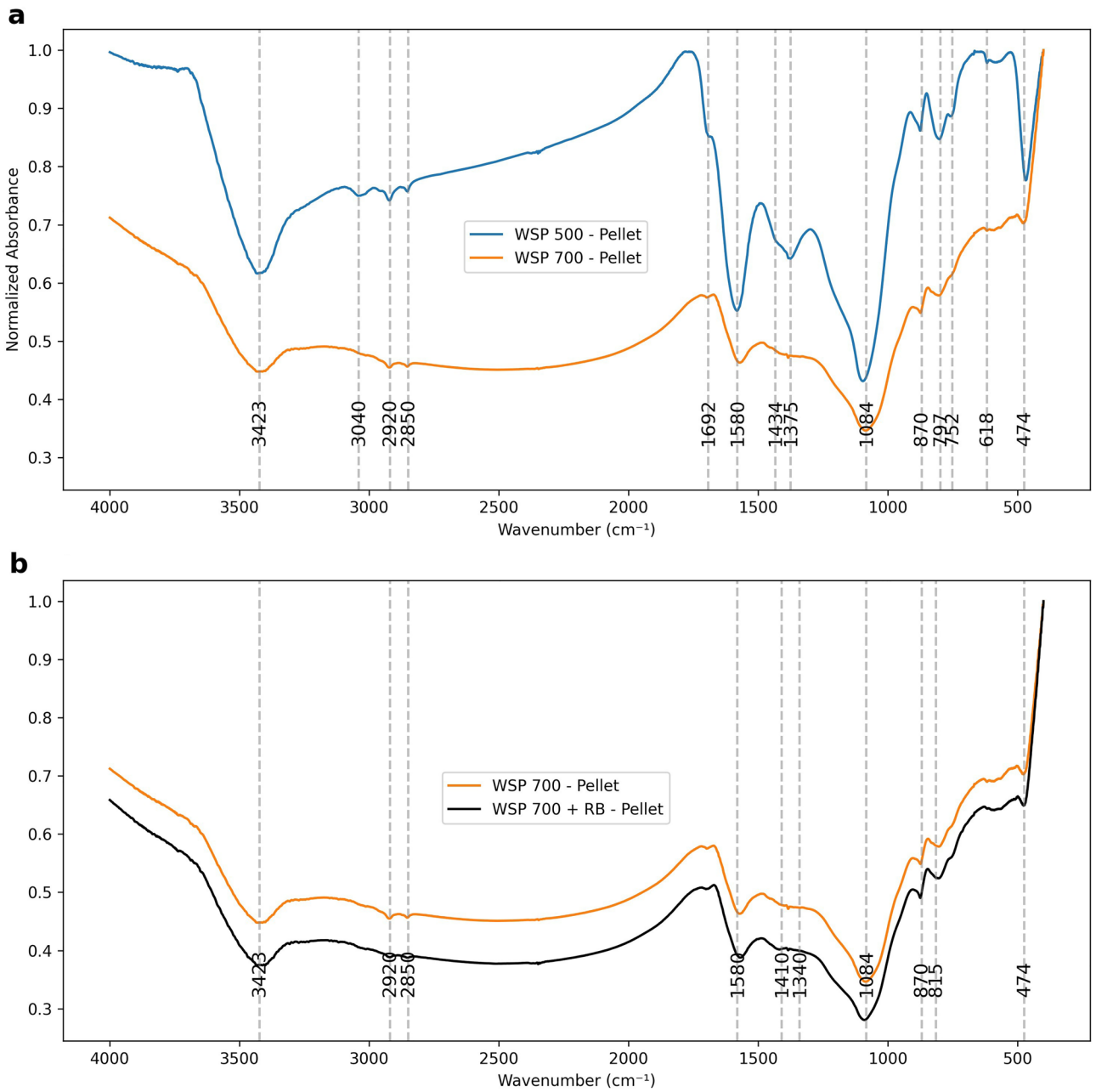

Fig. 9 **a** Comparative FT-IR spectra of WSP550 and WSP700 biochars; **b** FT-IR spectrum of WSP700 biochar before and after adsorption of RB5

rises, aligning with literature findings on the thermal degradation pathways of biomass components.

Regarding Fig. 9b, the bands around 2920 cm^{-1} and 2850 cm^{-1}, associated with C–H stretching vibrations from aliphatic groups (Aichour et al. 2019) diminished after the adsorption of RB5, indicating that these groups, present in the dye alone, may be involved in its interaction with the biochar during the adsorption process, mainly through hydrophobic interactions and van der Waals forces (Wang et al. 2024; Liu et al. 2025; Gupta et al. 2025), which help stabilize the dye on the surface. Hydrophobic interactions arise from the tendency of nonpolar regions of the dye and biochar to aggregate in water, minimizing contact with the aqueous medium, while van der Waals forces result from weak, non-specific attractions between closely approaching molecules, further aiding retention of RB5.

As discussed, although the PSO model fits the kinetic data, its applicability has limitations, particularly for heterogeneous surfaces or systems where mass transfer is significant. In this study, the adsorption mechanism appears to be dominated by electrostatic interactions between the negatively charged sulfonate groups of RB5 and the positively

Table 9 The mean effective concentrations for 50% of the organisms were calculated as percentages and toxic units for each sample

Effluent	EC50 (%)	TU
URE	1.146 (0.798–1.266)	87.26
TRE	2.151 (1.666–2.450)	46.42

The confidence interval was set at 95%. *URE* untreated real effluent, *TRE* treated real effluent, *TU* toxic unit

charged sites on the biochar surface, particularly under acidic to neutral conditions. These interactions explain the pH-dependent adsorption behavior, while the physical interactions from C–H groups support dye retention by promoting close contact with the adsorbent surface.

Ecotoxicological Results

The cladoceran *Daphnia similis* was utilized to establish a toxicity relationship between pre- and post-treatment samples for a pivotal model organism in ecotoxicology. This microcrustacean plays a fundamental role in the aquatic food chain (Altshuler et al. 2011) and its use in acute toxicity tests is standardized by several protocols (e.g. ABNT 2022; OECD 2012).

The synthetic solution prepared with RB5 alone exhibited an $EC_{50\text{-}48\,h}$ of 69.10 mg L^{-1} (95% CI: 61.92–73.76 mg L^{-1}) for *Daphnia similis* (Fig. S19-S21). After treatment, the survival rate of *Daphnia* exposed to 100% of the treated sample (concentration of 60 mg L^{-1}) was 55%. In dilute samples (10% of the treated effluent), the residual RB5 concentration was approximately 8.4 mg L^{-1}, which is below the EC_{50} determined for the synthetic solution. For the textile effluent samples containing the reactive dye, the $EC_{50\text{-}48\,h}$ values–both before and after biochar treatment–are presented in Table 9.

The differences observed in ecotoxicity outcomes between synthetic and real effluent samples can be attributed to the presence of a variety of auxiliary substances used during the dyeing process. These include humectants, detergents, stabilizers, and bleaching agents (Text S1), which are known to contribute to the overall toxicity of the effluent. Despite the differences between real and synthetic matrices, the results clearly indicate a reduction in toxicity after treatment, as evidenced by an increase in EC_{50} values and a corresponding decrease in the TU index. This demonstrates the effectiveness of the treatment in mitigating ecotoxicological effects.

The URE used in this study exhibited higher toxicity compared to values reported in the literature. Castro et al. (2019) reported EC_{50} values of 35.39% and 24.18% after 24 and 48 h of exposure, respectively, using various aquatic test organisms. In contrast, the untreated effluent in our study demonstrated greater acute toxicity towards *D. magna*. Similarly, Verma (2008) reported EC_{50}-48 h values of 55.32 mg L^{-1} and 46.84 mg L^{-1} for *D. magna* exposed Remazol Parrot Green and Remazol Golden Yellow, respectively. For three dye industry effluents (D1, D2, D3), EC_{50} values were 14.12%, 15.52%, and 29.69%, indicating significant toxicity. Textile mill effluents (T1, T2, T3) exhibited EC_{50} values of > 100%, 62.97%, and 63.04%, suggesting a comparatively lower toxicity than dye effluents.

Garcia et al., (2021) compared the toxicity of reactive dye RR239 and real textile effluents using different test organisms. Their study highlighted marked differences in toxicity between synthetic dyes and actual effluents. While *Vibrio fischeri* showed an EC_{50} of 10.14 ± 1.76 mg L^{-1} for RR239, *Daphnia similis* exhibited a significantly higher EC_{50} of 389.42 ± 3.77 mg L^{-1}. In tests using *Biomphalaria glabrata*, the EC_{50} for adult snails was 517.19 mg L^{-1}, while embryo EC_{50} values ranged from 116.41 mg L^{-1} (gastrula stage) to 124.14 mg L^{-1} (blastula stage). However, for real effluents, EC_{50} values for all tested organisms were below 15%, emphasizing the substantial toxicity of untreated textile wastewater.

Conclusions

This study evaluates the performance of WSP700 and OSR700 biochars for RB5 dye removal from synthetic and real textile effluents. WSP700 demonstrated superior adsorption capacity and faster kinetics compared to OSR700, following PSO kinetics, which indicates chemisorption as the dominant mechanism. The adsorption process was well-described by the Langmuir isotherm, suggesting monolayer adsorption, with WSP700 showing a higher q_{max}. Desorption tests revealed effective regeneration using Na_2CO_3, with only a slight reduction in efficiency after seven cycles. Coexisting ions in real effluent did not significantly affect RB5 adsorption, and WSP700 maintained its performance in both synthetic and real effluents, achieving a 32.65% removal efficiency in real effluent application. SEM and FT-IR analyses confirmed surface changes post-adsorption, highlighting interactions between the dye and biochar. Ecotoxicological testing showed a reduction in toxicity, further supporting WSP700's potential as an effective, sustainable, and reusable adsorbent for dye-contaminated wastewater treatment.

Despite these promising results, some limitations should be acknowledged. The adsorption capacities observed are moderate compared to commercial activated carbons, and equilibrium times were relatively long (up to 480 min), which may limit large-scale applications. In addition, the study was conducted under controlled laboratory conditions,

and long-term performance in continuous flow systems remains to be evaluated. Future studies should focus on scaling-up, surface modification strategies to enhance adsorption capacity, and the assessment of adsorption performance in effluents containing a wider variety of competing pollutants. Integrating biochar with hybrid treatment technologies could also provide synergistic effects, improving both efficiency and operational feasibility.

Supplementary Information The online version contains supplementary material available at https://doi.org/10.1007/s41742-025-01010-3.

Acknowledgements The authors would like to thank the Brazilian National Nuclear Energy Commission (CNEN-SP) for supporting this study, Dr. Ondrej Masek from the Biochar Research Centre (UKBRC, University of Edinburgh, UK) for supplying the standard biochars, and Mr. Jorge Marcos Rosa from the SENAI Institute of Technology for providing the dye and formulating the real effluent containing the dye. The authors also express their gratitude to Mr. Milton Faria Diniz, from the Institute of Aeronautics and Space (DCTA/IAE), for performing the FT-IR analyses and to all colleagues and collaborators who contributed to the successful completion of this work.

Authors Contributions SNG: Conceptualization, Funding acquisition, Methodology, Supervision, Writing – original draft, Writing – review and editing; TTS: Data curation, Investigation, Formal analysis, Methodology, Writing – original draft; GEZS: Data curation, Investigation; SIB: Resources, Writing – review and editing; LGA: Conceptualization, Data curation, Formal analysis, Investigation, Methodology, Visualization, Writing – original draft, Writing – review & editing.

Funding The authors declare that no funds, grants, or other support were received during the preparation of this manuscript.

Data Availability All data generated or analyzed during this study are included in this published article and its Supplementary Information files. Should any raw data files be needed in another format they are available from the corresponding author upon reasonable request.

Declarations

Conflict of interest The authors have no relevant financial or non-financial interests to disclose.

Ethical approval Not applicable.

Consent to participate Not applicable.

Consent to publish Not applicable.

References

Abdu M, Babaee S, Worku A et al (2024) The development of giant reed biochar for adsorption of Basic Blue 41 and Eriochrome Black T. azo dyes from wastewater. Sci Rep 14:18320. https://doi.org/10.1038/s41598-024-67997-5

ABNT (2009) Ecotoxicologia aquática–Toxicidade aguda–Método de ensaio com *Daphnia* spp. Cladócera Crustácea 12713:23

ABNT (2022) NBR 12713: Ecotoxicologia aquática: toxicidade aguda - método de ensaio com *Daphnia* spp (Cladocera, Crustacea), Quinta edição. ABNT, Rio de Janeiro - RJ

Ahmad M, Lee SS, Dou X et al (2012) Effects of pyrolysis temperature on soybean stover- and peanut shell-derived biochar properties and TCE adsorption in water. Bioresour Technol 118:536–544. https://doi.org/10.1016/j.biortech.2012.05.042

Ahmad N, Suryani Arsyad F, Royani I, Lesbani A (2022) Adsorption of methylene blue on magnetite humic acid: kinetic, isotherm, thermodynamic, and regeneration studies. Results Chem 4:100629. https://doi.org/10.1016/j.rechem.2022.100629

Aichour A, Zaghouane-Boudiaf H, Mohamed Zuki FB et al (2019) Low-cost, biodegradable and highly effective adsorbents for batch and column fixed bed adsorption processes of methylene blue. J Environ Chem Eng 7:103409. https://doi.org/10.1016/j.jece.2019.103409

Aksu Z, Akın AB (2010) Comparison of Remazol Black B biosorptive properties of live and treated activated sludge. Chem Eng J 165:184–193. https://doi.org/10.1016/j.cej.2010.09.014

Aksu Z, Tezer S (2000) Equilibrium and kinetic modelling of biosorption of Remazol Black B by *Rhizopus arrhizus* in a batch system: effect of temperature. Process Biochem 36:431–439. https://doi.org/10.1016/S0032-9592(00)00233-8

Alaguprathana M, Poonkothai M (2021) Haematological, biochemical, enzymological and histological responses of *Labeo rohita* exposed to methyl orange dye solution treated with *Oedogonium subplagiostomum* AP1. Environ Sci Pollut Res 28:17602–17612. https://doi.org/10.1007/s11356-020-12208-7

Altshuler I, Demiri B, Xu S et al (2011) An integrated multi-disciplinary approach for studying multiple stressors in freshwater ecosystems: *daphnia* as a model organism. Integr Comp Biol 51:623–633. https://doi.org/10.1093/icb/icr103

Amini M, Younesi H, Bahramifar N et al (2008) Application of response surface methodology for optimization of lead biosorption in an aqueous solution by *Aspergillus niger*. J Hazard Mater 154:694–702. https://doi.org/10.1016/j.jhazmat.2007.10.114

Arafat Hossain M, Ganesan P, Jewaratnam J, Chinna K (2017) Optimization of process parameters for microwave pyrolysis of oil palm fiber (OPF) for hydrogen and biochar production. Energy Convers Manag 133:349–362. https://doi.org/10.1016/j.enconman.2016.10.046

Aranda-García E, Chávez-Camarillo GMa, Cristiani-Urbina E (2020) Effect of ionic strength and coexisting ions on the biosorption of divalent nickel by the acorn shell of the oak *Quercus crassipes* Humb. & Bonpl. Processes 8:1229. https://doi.org/10.3390/pr8101229

Arif M, Liu G, Zia-ur-Rehman M et al (2025) High-performance clay and K_2CO_3-modified sludge biochar for efficient reactive black-5 removal: mechanistic insights and alleviation of phytotoxicity. Biomass Bioenergy 202:108235. https://doi.org/10.1016/j.biombioe.2025.108235

Ashori A, Hamzeh Y, Azadeh E et al (2012) Potential of canola stalk as biosorbent for the removal of remazol black b reactive dye from aqueous solutions. J Wood Chem Technol 32:328–341. https://doi.org/10.1080/02773813.2012.688912

Baudrot V, Charles S (2021) morse: an R-package to analyse toxicity test data. J Open Source Softw 6:3200. https://doi.org/10.21105/joss.03200

Behnamfard A, Salarirad MM (2009) Equilibrium and kinetic studies on free cyanide adsorption from aqueous solution by activated carbon. J Hazard Mater 170:127–133. https://doi.org/10.1016/j.jhazmat.2009.04.124

Cao X, Ma L, Gao B, Harris W (2009) Dairy-manure derived biochar effectively sorbs lead and atrazine. Environ Sci Technol 43:3285–3291. https://doi.org/10.1021/es803092k

Cardoso NF, Pinto RB, Lima EC et al (2011) Removal of remazol black B textile dye from aqueous solution by adsorption. Desalination 269:92–103. https://doi.org/10.1016/j.desal.2010.10.047

Castro AM, Nogueira V, Lopes I et al (2019) Evaluation of the potential toxicity of effluents from the textile industry before and after treatment. Appl Sci 9:3804. https://doi.org/10.3390/app9183804

Cavalcante LC, De Carvalho KQ, Bassetti FJ, Coral LAA (2024) Kinetic, isothermal and thermodynamic studies of Reactive Black 5 removal using rice husk ashes and powdered activated carbon. Desalin Water Treat 320:100606. https://doi.org/10.1016/j.dwt.2024.100606

Chen A-H, Chen S-M (2009) Biosorption of azo dyes from aqueous solution by glutaraldehyde-crosslinked chitosans. J Hazard Mater 172:1111–1121. https://doi.org/10.1016/j.jhazmat.2009.07.104

Chen A-H, Huang Y-Y (2010) Adsorption of Remazol Black 5 from aqueous solution by the templated crosslinked-chitosans. J Hazard Mater 177:668–675. https://doi.org/10.1016/j.jhazmat.2009.12.083

Chen W, Parette R, Zou J et al (2007) Arsenic removal by iron-modified activated carbon. Water Res 41:1851–1858. https://doi.org/10.1016/j.watres.2007.01.052

Chowdhury S, Chakraborty S, Saha P (2011) Biosorption of Basic Green 4 from aqueous solution by *Ananas comosus* (pineapple) leaf powder. Colloids Surf B Biointerfaces 84:520–527. https://doi.org/10.1016/j.colsurfb.2011.02.009

Claus C (1876) Zur Kenntnis der Organisation und des feinern Baues der Daphniden und verwandter Cladoceren. Zeitschrift für wissenschaftliche Zoologie

Ćwieląg-Piasecka I, Jamroz E, Medyńska-Juraszek A et al (2023) Deashed wheat-straw biochar as a potential superabsorbent for pesticides. Materials 16:2185. https://doi.org/10.3390/ma16062185

da Fontoura JT, Rolim GS, Mella B et al (2017) Defatted microalgal biomass as biosorbent for the removal of Acid Blue 161 dye from tannery effluent. J Environ Chem Eng 5:5076–5084. https://doi.org/10.1016/j.jece.2017.09.051

Dallago RM, Smaniotto A, de Oliveira LCA (2005) Solid waste from tanneries as adsorbent for the removal of dyes in aqueous medium. Quim Nova 28:433–437. https://doi.org/10.1590/S0100-40422005000300013

De Araujo LG, Vilcocq L, Fongarland P, Schuurman Y (2025) Recent developments in the use of machine learning in catalysis: a broad perspective with applications in kinetics. Chem Eng J 508:160872. https://doi.org/10.1016/j.cej.2025.160872

Donnaperna L, Duclaux L, Gadiou R et al (2009) Comparison of adsorption of Remazol Black B and Acidol Red on microporous activated carbon felt. J Colloid Interface Sci 339:275–284. https://doi.org/10.1016/j.jcis.2009.07.057

Dursun AY, Tepe O, Uslu G et al (2013) Kinetics of remazol black B adsorption onto carbon prepared from sugar beet pulp. Environ Sci Pollut Res 20:2472–2483. https://doi.org/10.1007/s11356-012-1133-4

El Idrissi M, Elharfaoui S, Zmirli Z et al (2024) Theoretical and experimental study of the orientation to the most effective coagulant for removing Reactive Black-5 dye from industrial effluents. Phys Chem Res 12(1):229–248

Elnour AY, Alghyamah AA, Shaikh HM et al (2019) Effect of pyrolysis temperature on biochar microstructural evolution, physicochemical characteristics, and its influence on biochar/polypropylene composites. Appl Sci 9:1149. https://doi.org/10.3390/app9061149

Elwakeel KZ (2009) Removal of reactive black 5 from aqueous solutions using magnetic chitosan resins. J Hazard Mater 167:383–392. https://doi.org/10.1016/j.jhazmat.2009.01.051

Faria PCC, Orfão JJM, Pereira MFR (2004) Adsorption of anionic and cationic dyes on activated carbons with different surface chemistries. Water Res 38:2043–2052. https://doi.org/10.1016/j.watres.2004.01.034

Feng L, Liu J, Guo Z et al (2022) Reactive black 5 dyeing wastewater treatment by electrolysis-Ce (IV) electrochemical oxidation technology: influencing factors, synergy and enhancement mechanisms. Sep Purif Technol 285:120314. https://doi.org/10.1016/j.seppur.2021.120314

Fu S, Di J, Guo X et al (2023) Preparation of lignite-loaded nano-FeS and its performance for treating acid Cr(VI)-containing wastewater. Environ Sci Pollut Res 30:3351–3366. https://doi.org/10.1007/s11356-022-22411-3

Garcia VSG, De Freitas Tallarico L, Rosa JM et al (2021) Multiple adverse effects of textile effluents and reactive Red 239 dye to aquatic organisms. Environ Sci Pollut Res 28:63202–63214. https://doi.org/10.1007/s11356-021-15115-7

Goswami L, Kushwaha A, Kafle SR, Kim B-S (2022) Surface modification of biochar for dye removal from wastewater. Catalysts 12:817. https://doi.org/10.3390/catal12080817

Guaratini CCI, Zanoni MVB (2000) Corantes Têxteis. Quím Nova 23:71–78. https://doi.org/10.1590/S0100-40422000000100013

Gupta A, Ramachandran S, Mayilswamy N et al (2025) Dye-laden sludge-derived biochar for wastewater remediation: a review on pyrolytic engineering, adsorptive interactions, and environmental prospects. Sustain Chem Environ 11:100271. https://doi.org/10.1016/j.scenv.2025.100271

Guy M, Mathieu M, Anastopoulos IP et al (2022) Process parameters optimization, characterization, and application of KOH-activated Norway spruce bark graphitic biochars for efficient azo dye adsorption. Molecules 27:456. https://doi.org/10.3390/molecules27020456

Hamzeh Y, Ashori A, Azadeh E, Abdulkhani A (2012) Removal of Acid Orange 7 and Remazol Black 5 reactive dyes from aqueous solutions using a novel biosorbent. Mater Sci Eng C Mater Biol 32:1394–1400. https://doi.org/10.1016/j.msec.2012.04.015

Hubbe M, Azizian S, Douven S (2019) Implications of apparent pseudo-second-order adsorption kinetics onto cellulosic materials: a review. BioResources 14:7582–7626. https://doi.org/10.15376/biores.14.3.7582-7626

Kalderis D, Kotti MS, Méndez A, Gascó G (2014) Characterization of hydrochars produced by hydrothermal carbonization of rice husk. Solid Earth 5:477–483. https://doi.org/10.5194/se-5-477-2014

Karakoyun N, Kubilay S, Aktas N et al (2011) Hydrogel-Biochar composites for effective organic contaminant removal from aqueous media. Desalination 280:319–325. https://doi.org/10.1016/j.desal.2011.07.014

Karaman C, Aksu Z (2020) Modelling of Remazol Black-B adsorption on chemically modified waste orange peel: pH shifting effect of acidic treatment. Sakarya Univ J Sci 24:1135–1150. https://doi.org/10.16984/saufenbilder.751491

Kauwe SK, Graser J, Murdock R, Sparks TD (2020) Can machine learning find extraordinary materials? Comput Mater Sci 174:109498. https://doi.org/10.1016/j.commatsci.2019.109498

Kong L, Liu G (2021) Synchrotron-based infrared microspectroscopy under high pressure: an introduction. Matter Radiat Extremes 6:068202. https://doi.org/10.1063/5.0071856

Krishna Moorthy A, Govindarajan Rathi B, Shukla SP et al (2021) Acute toxicity of textile dye Methylene blue on growth and metabolism of selected freshwater microalgae. Environ Toxicol Pharmacol 82:103552. https://doi.org/10.1016/j.etap.2020.103552

Krstić V (2021) Chapter 14 - Role of zeolite adsorbent in water treatment. In: Bhanvase B, Sonawane S, Pawade V, Pandit A (eds) Handbook of nanomaterials for wastewater treatment. Elsevier, pp 417–481

Kuo C-Y, Wu C-H, Wu J-Y (2008) Adsorption of direct dyes from aqueous solutions by carbon nanotubes: determination of equilibrium,

kinetics and thermodynamics parameters. J Colloid Interface Sci 327:308–315. https://doi.org/10.1016/j.jcis.2008.08.038

Leal CC, da Rocha ORS, Duarte MM, et al (2010) Evaluation of the adsorption process of remazol black B dye in liquid effluents by green coconut mesocarp. Afinidad J Chem Eng Theor Appl Chem 67.

Leal ANR, De Lima ADCA, Azevedo MGFDA, et al (2021) Removal of Remazol Black B dye using bacterial cellulose as an adsorbent. Sci Plena. https://doi.org/10.14808/sci.plena.2021.034201

Lee YH, Pavlostathis SG (2004) Decolorization and toxicity of reactive anthraquinone textile dyes under methanogenic conditions. Water Res 38:1838–1852. https://doi.org/10.1016/j.watres.2003.12.028

Lestari DY, Laksono EW, Ikhsan J, Rohaeti E (2023) Modified natural zeolite as adsorbent for remazol black b dye: Kinetics and equilibrium aspects. Bhubaneswar, India, p 040011

Liu C, Balasubramanian P, Nguyen XC et al (2025) Enhanced machine learning prediction of biochar adsorption for dyes: parameter optimization and experimental validation. Carbon Res 4:46. https://doi.org/10.1007/s44246-025-00213-9

Lu H, Zhang W, Yang Y et al (2012) Relative distribution of Pb^{2+} sorption mechanisms by sludge-derived biochar. Water Res 46:854–862. https://doi.org/10.1016/j.watres.2011.11.058

Luan J, Hou P-X, Liu C et al (2016) Efficient adsorption of organic dyes on a flexible single-wall carbon nanotube film. J Mater Chem A 4:1191–1194. https://doi.org/10.1039/C5TA08627B

Manna S, Singh N, Purakayastha TJ, Berns AE (2020) Effect of deashing on physico-chemical properties of wheat and rice straw biochars and potential sorption of pyrazosulfuron-ethyl. Arab J Chem 13:1247–1258. https://doi.org/10.1016/j.arabjc.2017.10.005

Mohan D, Sarswat A, Ok YS, Pittman CU (2014) Organic and inorganic contaminants removal from water with biochar, a renewable, low cost and sustainable adsorbent–a critical review. Bioresour Technol 160:191–202. https://doi.org/10.1016/j.biortech.2014.01.120

Mokue Mafo SG, Nanssou Kouteu PA, Tchuifon Tchuifon DR et al (2025) Low-cost magnetic carbons-based rubber seed husks materials for highly efficient removal for reactive black 5 and reactive blue 19 textile dyes from wastewater. Int J Environ Anal Chem 105:701–725. https://doi.org/10.1080/03067319.2023.2269857

Nakagawa K, Namba A, Mukai SR et al (2004) Adsorption of phenol and reactive dye from aqueous solution on activated carbons derived from solid wastes. Water Res 38:1791–1798. https://doi.org/10.1016/j.watres.2004.01.002

Neusatz Guilhen S, Watanabe T, Tieko Silva T et al (2022) Role of point of zero charge in the adsorption of cationic textile dye on standard biochars from aqueous solutions: selection criteria and performance assessment. Recent Prog Mater 4:1–30. https://doi.org/10.21926/rpm.2202010

Nigam P, Banat IM, Singh D, Marchant R (1996) Microbial process for the decolorization of textile effluent containing azo, diazo and reactive dyes. Process Biochem 31:435–442. https://doi.org/10.1016/0032-9592(95)00085-2

OECD (2012) Test No. 211: *Daphnia magna* reproduction test. OECD Publishing.

Oliveira DP de (2005) Corantes como importante classe de contaminantes ambientes - um estudo de caso. Tese de Doutorado, Faculdade de Ciências Farmacêuticas, Universidade de São Paulo, São Paulo. https://doi.org/10.11606/T.9.2005.tde-18092007-101040

Prabhakar N, Isloor AM, Padaki M, Fauzi Ismail A (2024) Fabrication of TiO_2@ZIF-67 metal organic framework composite incorporated PVDF membranes for the removal of hazardous reactive black 5 and Congo red dyes from contaminated water. Chem Eng J 498:155270. https://doi.org/10.1016/j.cej.2024.155270

Qayyum MF, Steffens D, Reisenauer HP, Schubert S (2012) Kinetics of carbon mineralization of biochars compared with wheat straw in three soils. J Environ Qual 41:1210–1220. https://doi.org/10.2134/jeq2011.0058

Qian L, Chen B (2013) Dual role of biochars as adsorbents for aluminum: the effects of oxygen-containing organic components and the scattering of silicate particles. Environ Sci Technol 47:8759–8768. https://doi.org/10.1021/es401756h

Ríos F, Fernández-Arteaga A, Lechuga M, Fernández-Serrano M (2017) Ecotoxicological characterization of polyoxyethylene glycerol ester non-ionic surfactants and their mixtures with anionic and non-ionic surfactants. Environ Sci Pollut Res Int 24:10121–10130. https://doi.org/10.1007/s11356-017-8662-9

Rodrigues LA, da Silva MLCP, Alvarez-Mendes MO et al (2011) Phenol removal from aqueous solution by activated carbon produced from avocado kernel seeds. Chem Eng J 174:49–57. https://doi.org/10.1016/j.cej.2011.08.027

Rubin E, Rodriguez P, Herrero R, de Sastre Vicente Me (2006) Biosorption of phenolic compounds by the brown alga *Sargassum muticum*. Adsorption 81:1093–1099. https://doi.org/10.1002/jctb.1430

Rubio-Clemente A, Gutiérrez J, Henao H et al (2023) Adsorption capacity of the biochar obtained from *Pinus patula* wood microgasification for the treatment of polluted water containing malachite green dye. J King Saud Univ Eng Sci 35:431–441. https://doi.org/10.1016/j.jksues.2021.07.006

Sari A, Sari F (2021) A comparative examination of acute toxicities of three disazo dyes to freshwater macroinvertebrates *Gammarus roeseli* (Crustacea: Amphipoda) and *Chironomus riparius* (Insecta: Diptera). Chem Ecol 37:683–703. https://doi.org/10.1080/02757540.2021.1974008

Şen S, Korkmaz F, Kiliç NK (2025) Biosorption of reactive dyes by novel bacterium *Leclercia adecarboxylata*: complete removal of Reactive Black 5 and molecular insights into the adsorption mechanism. Water Environ Res 97:e70109. https://doi.org/10.1002/wer.70109

Senturk HB, Ozdes D, Gundogdu A et al (2009) Removal of phenol from aqueous solutions by adsorption onto organomodified Tirebolu bentonite: equilibrium, kinetic and thermodynamic study. J Hazard Mater 172:353–362. https://doi.org/10.1016/j.jhazmat.2009.07.019

Shen Y-S, Wang S-L, Tzou Y-M et al (2012) Removal of hexavalent Cr by coconut coir and derived chars--the effect of surface functionality. Bioresour Technol 104:165–172. https://doi.org/10.1016/j.biortech.2011.10.096

Silva TC, Fraga TJM, Carvalho M et al (2018) Removal of the reactive Remazol Black B and Remazol Red from aqueous solutions by adsorption onto treated residue from the aluminum industry. Latin American Appl Res - an Int J 48:101–106. https://doi.org/10.52292/j.laar.2018.266

Silva TT, Jacinavicius FR, Pinto E, Borrely SI (2023) Intracellular microcystins degradation and acute toxicity decrease towards *Daphnia similis* by low electron-beam irradiation doses. Algal Res 72:103086. https://doi.org/10.1016/j.algal.2023.103086

Singh A, Mittal A, Jangid NK (2020) Toxicology of Dyes: In: Wani KA, Jangid NK, Bhat AR (eds) Advances in Human Services and Public Health. IGI Global, pp 50–69

Soares JL (1998) Remoção de corantes têxteis por adsorção em carvão mineral ativado com alto teor de cinzas /

Sun L, Wan S, Luo W (2013) Biochars prepared from anaerobic digestion residue, palm bark, and eucalyptus for adsorption of cationic methylene blue dye: characterization, equilibrium, and kinetic studies. Bioresour Technol 140:406–413. https://doi.org/10.1016/j.biortech.2013.04.116

Tunç Ö, Tanacı H, Aksu Z (2009) Potential use of cotton plant wastes for the removal of Remazol Black B reactive dye. J Hazard Mater 163:187–198. https://doi.org/10.1016/j.jhazmat.2008.06.078

Tuzen M, Sari A, Mendil D et al (2009) Characterization of biosorption process of As(III) on green algae *Ulothrix cylindricum*. J Hazard Mater 165:566–572. https://doi.org/10.1016/j.jhazmat.2008.10.020

Vaghela DR, Pawar A, Sharma D (2023) Effectiveness of wheat straw biochar in aqueous Zn removal: correlation with biochar characteristics and optimization of process parameters. Bioenerg Res 16:457–471. https://doi.org/10.1007/s12155-022-10471-9

Verma Y (2008) Acute toxicity assessment of textile dyes and textile and dye industrial effluents using *Daphnia magna* bioassay. Toxicol Ind Health 24:491–500. https://doi.org/10.1177/0748233708095769

Vijayaraghavan K, Yun Y-S (2008a) Bacterial biosorbents and biosorption. Biotechnol Adv 26:266–291. https://doi.org/10.1016/j.biotechadv.2008.02.002

Vijayaraghavan K, Yun Y-S (2008b) Biosorption of C.I. reactive black 5 from aqueous solution using acid-treated biomass of brown seaweed *Laminaria* sp. Dyes Pigments 76:726–732. https://doi.org/10.1016/j.dyepig.2007.01.013

Wang Y-S, Huo T-R, Wang Y et al (2024) Constructing mesoporous biochar derived from waste carton: improving multi-site adsorption of dye wastewater and investigating mechanism. Environ Res 242:117775. https://doi.org/10.1016/j.envres.2023.117775

Watanabe T, Guilhen SN, Marumo JT et al (2022) Uranium biosorption by hydroxyapatite and bone meal: evaluation of process variables through experimental design. Environ Sci Pollut Res Int 29:79816–79829. https://doi.org/10.1007/s11356-021-17551-x

Wawrzkiewicz M, Hubicki Z (2011) Remazol black B removal from aqueous solutions and wastewater using weakly basic anion exchange resins. Open Chem 9:867–876. https://doi.org/10.2478/s11532-011-0072-0

Xu X, Cao X, Zhao L (2013) Comparison of rice husk- and dairy manure-derived biochars for simultaneously removing heavy metals from aqueous solutions: role of mineral components in biochars. Chemosphere 92:955–961. https://doi.org/10.1016/j.chemosphere.2013.03.009

Xue Y, Gao B, Yao Y et al (2012) Hydrogen peroxide modification enhances the ability of biochar (hydrochar) produced from hydrothermal carbonization of peanut hull to remove aqueous heavy metals: batch and column tests. Chem Eng J 200–202:673–680. https://doi.org/10.1016/j.cej.2012.06.116

Yagub MT, Sen TK, Afroze S, Ang HM (2014) Dye and its removal from aqueous solution by adsorption: a review. Adv Colloid Interface Sci 209:172–184. https://doi.org/10.1016/j.cis.2014.04.002

Yang Y, Wei Z, Zhang X et al (2014) Biochar from *Alternanthera philoxeroides* could remove Pb(II) efficiently. Bioresour Technol 171:227–232. https://doi.org/10.1016/j.biortech.2014.08.015

Yao Y, Gao B, Chen H et al (2012) Adsorption of sulfamethoxazole on biochar and its impact on reclaimed water irrigation. J Hazard Mater 209–210:408–413. https://doi.org/10.1016/j.jhazmat.2012.01.046

Zhang M, Gao B, Yao Y et al (2012) Synthesis of porous MgO-biochar nanocomposites for removal of phosphate and nitrate from aqueous solutions. Chem Eng J 210:26–32. https://doi.org/10.1016/j.cej.2012.08.052

Zhang X, Wang H, He L et al (2013) Using biochar for remediation of soils contaminated with heavy metals and organic pollutants. Environ Sci Pollut Res Int 20:8472–8483. https://doi.org/10.1007/s11356-013-1659-0

Zhang Z, Huang G, Zhang P et al (2023) Development of iron-based biochar for enhancing nitrate adsorption: effects of specific surface area, electrostatic force, and functional groups. Sci Total Environ 856:159037. https://doi.org/10.1016/j.scitotenv.2022.159037

Zheng W, Guo M, Chow T et al (2010) Sorption properties of greenwaste biochar for two triazine pesticides. J Hazard Mater 181:121–126. https://doi.org/10.1016/j.jhazmat.2010.04.103

Ziapour A, Sefidrooh M, Moadeli M (2016) Adsorption of remazol black b dye from aqueous solution using bagasse. Prog Color Color Coat 9:99–108